THE IMPACT OF HUMAN IMMUNODEFICIENCY VIRUS (HIV) ANTIRETROVIRAL DRUG EXPOSURE *IN-UTERO* ON LATER FERTILITY

By

Saba Zafar

Bachelor of Science (Honours), Ryerson University, 2018

A thesis

presented to Ryerson University

in partial fulfillment of the

requirements for the degree of

Master of Science

in the program of

Molecular Science

Toronto, Ontario, Canada, 2020

AUTHORS DECLARATION FOR ELECTRONIC SUBMISSION OF A THESIS:

I hereby declare that I am the sole author of this thesis. This is a true copy of the thesis, including any required final revisions, as accepted by my examiners.

I authorize Ryerson University to lend this thesis to other institutions or individuals for the purpose of scholarly research.

I further authorize Ryerson University to reproduce this thesis by photocopying or by other means, in total or in part, at the request of other institutions or individuals for the purpose of scholarly research.

I understand that my thesis may be made electronically available to the public.

THE IMPACT OF HUMAN IMMUNODEFICIENCY VIRUS (HIV) ANTIRETROVIRAL DRUG EXPOSURE *IN-UTERO* ON LATER FERTILITY

Saba Zafar, Master of Science, Molecular Science. Ryerson University, 2020.

ABSTRACT:

Combination antiretroviral therapy (cART) reduces the risk of vertical human immunodeficiency virus (HIV) transmission. Two nucleoside reverse transcriptase inhibitors (NRTIs) are usually included in cART. The efficacy of cART has been extensively studied, but a significant knowledge gap exists concerning the effects of *in-utero* exposure on developing fetuses. **In this project, we assessed the effects of HIV antiretrovirals on the reproductive health of offspring.** Using *Schizosaccharomyces pombe*, we have shown that mutagenicity, but not toxicity, increases over time after dual-NRTI exposure. Our mouse pregnancy model suggests that *in-utero* cART exposure does not affect female germ cell development but alters the testes structure, thus adversely impacting male germ cell development. However, our study is limited in sample size and we aim to improve this by quantifying more gonad sections. Ultimately, we hope to provide more insight on the potential long-term fertility issues faced by children exposed *in-utero* to antiretrovirals.

ACKNOWLEDGEMENTS:

I thank my supervisors Dr. Sarah Sabatinos and Dr. Lena Serghides for their support, enthusiasm and guidance both in and out of the lab. I am grateful for all that I have learned under their mentorships. I am also thankful to my committee member Dr. Martina Hausner for her helpful recommendations and support. Pursuing this degree would not nearly have been as enjoyable without the encouragement and humor of my lab mates and colleagues in the Molecular Science program. I would like to thank all Sabatinos lab members, especially Mahsa Paydarnia and Ethan Francis for their assistance with experiments, as well as all Serghides lab members, especially Mónica Guzmán Lenis and Smriti Kala for their guidance and help with experimental protocols. I also thank Ella Hyatt and Sarah Kovacs for providing valuable information and administrative support. Lastly, I thank my family and friends for being a constant source of support, sheer positivity and quality memes.

Table of Contents

LIST OF TABLES:

LIST OF FIGURES:

LIST OF ABBREVIATIONS:

2',3'-dideoxyinosine (ddI)

5-bromo-29-deoxyuridine (BrdU)

5-ethynyl-29-deoxyuridine (EdU)

Abacavir (ABC)

Acquired immune deficiency syndrome (AIDS)

Androgen-binding protein (ABP)

Azidothymidine (AZT)

Combination antiretroviral therapy (cART)

Combivir (AZT/3TC)

Cytosine (C)

Cytosine-Guanine dinucleotide (CpG)

DdI (dideoxyinosine)

Deoxynucleotide triphosphates (dNTPs)

DNA methyltransferases (Dnmts)

DNA Synthesis phase (S-phase)

Double stranded breaks (DSBs)

Efavirenz (EFV)

Fluctuation Analysis Calculator (FALCOR)

Follicle-stimulating hormone (FSH)

Gap phase I (G1)

Gap phase II (G2)

Gestational day (GD)

Guanine (G)

Hematoxylin and Eosin (H&E)

Herpes simplex virus thymidine kinase (*hsv-tk*)

Human equilibrative nucleoside transporter 1 (*hENT1*)

Human Immunodeficiency Virus (HIV)

Hydroxyurea (HU)

Interleukin (IL)

Kaletra (ritonavir-boosted lopinavir)

Kivexa (ABC/3TC)

Lamivudine (3TC)

Luteinizing hormone (LH)

Mitosis phase (M-phase)

Mutation frequency (r/N_t)

Mutation rate (m/N_t)

Nucleoside reverse transcriptase inhibitors (NRTIs)

Number of mutants (r)

Number of mutational events (m)

Phosphate bond (p)

Pombe Glutamate Media with Histidine, Uracil, Leucine and Adenine (PMG-HULA)

Pombe Glutamate Media with Uracil and Adenine (PMG-UA)

Postnatal day (PND)

Ritonavir-boosted atazanavir (ATV/r)

Tenofovir disoproxil fumarate (TDF)

T-helper (TH)

Total number of viable cells (N_t)

University Health Network (UHN)

World Health Organization (WHO)

Yeast Extract with Supplement (YES)

1.0 INTRODUCTION

1.1 Overview of HIV:

1.1.1 What is HIV?

The Human Immunodeficiency Virus (HIV) is a type of lentivirus that attacks immune cells essential for the adaptive immune response. The lentivirus genus falls under the Retroviridae family. Lentiviruses share several clinical characteristics including long incubation times and suppression of the immune response. They also have clinical implications for the hematopoietic and central nervous systems. The nucleoid of lentivirus particles is cone-shaped and their envelope includes glycoproteins.[1] The *gag, pol* and *env* genes are found in the genome of all retroviruses. These genes code for structural proteins and enzymes necessary to the viral life cycle like reverse transcriptase, integrase, protease and RNase H. Additionally, the genome of lentiviruses also contains other regulatory genes necessary for viral persistence and spread.[2]

HIV targets CD4+ T-cells, microglia, monocytes and macrophages. The viral envelope glycoprotein gp120 interacts with the HLA class II receptor CD4 which facilitates viral entry. The viral enzyme reverse transcriptase converts the viral RNA to DNA, which is then integrated into the host cell's DNA by viral integrase. After DNA integration, the virus is considered a provirus and it can now use the host's genetic machinery to create RNA and proteins for the progeny virions, which will undergo new viral life cycles.[2] Low CD4+ T-cell counts are typically associated with HIV disease progression. An untreated HIV infection can lead to acquired immune deficiency syndrome (AIDS), which corresponds to less than 200 CD4+ T-cells per microlitre. AIDS and the associated loss of an effective immune response can increase the risk of opportunistic infections and viral induced cancers.[1]

1.1.2 HIV Transmission:

With approximately 38 million people living with HIV in the world, it is a significant global public health issue.[3] While the primary route for HIV infection is through sexual transmission, the virus can also spread by vertical transmission from mother to child.[4,5] This vertical transmission may occur *in utero* during the pregnancy, during birth or postpartum while breastfeeding, with developing fetuses infected *in utero* being at the highest risk for death.[6] In 2018, nearly 1.7 million children below the age of 15 were living with HIV, many of whom were infected through vertical transmission.[3,7]

1.2 Combination Antiretroviral Therapy (cART):

While a permanent cure for HIV does not exist, HIV infection can be treated with combination antiretroviral therapy (cART).[8] cART is comprised of at least three different anti-HIV drugs. This combination typically consists of two nucleoside reverse transcriptase inhibitors (NRTIs), plus either a protease inhibitor, a non-NRTI, or an integrase strand transfer inhibitor.[8,9] cART is highly efficacious at reducing virus levels by preventing HIV replication, and the efficacy of different cART regimens is well-studied.[8,10-11] In fact, the recent decline in mortality among people with HIV correlates with an increase in access to antiretroviral therapy.[12] In 2018, approximately 62% of adults and 54% of children (0-14 years of age) living with HIV had access to cART.[3] In 2018, an estimated 82% of pregnant women living with HIV in the world also had access to cART.[13]

1.2.1 NRTIs: The Backbones of cART:

Azidothymidine (3'-azido-3'deoxythymidine or AZT) and Lamivudine (2',3-dideoxy-3'-thiacytidine or 3TC) are NRTIs that have been used in cART since the mid-1990's (Figure 1).[14] AZT is a thymidine analogue while 3TC is a cytidine analogue.[15,16] In the 1980s, AZT was used as a monotherapy. Although the improvement in disease-progression was significant, there were concerns about its toxicity as side-effects included anemia, headaches, neutropenia, mitochondrial dysfunction and lipoatrophy.[17–19] The cytidine analog 3TC was considered less toxic than AZT, with minor side effects like headaches and insomnia.[17,18] The development of resistance mutations in the virus' reverse transcriptase lowered the efficacy of NRTI monotherapy.[18,20] The introduction of dual-therapy with AZT/3TC significantly reduced viral load and was less susceptible to detrimental resistance mutations than monotherapy. In comparison with AZT monotherapy, AZT/3TC dual-therapy was less toxic, although it is worth considering that AZT monotherapy was prescribed at higher doses and taken more frequently.[18] However, the efficacy of dual-NRTI therapy was short-term and the need for newer drugs remained. Other types of drugs like protease inhibitors were developed. Clinical trials that used AZT/3TC in combination with protease inhibitors showed short- and long-term viral suppression with improved clinical outcomes.[18,21,22] With NRTIs becoming the backbone of cART, the AZT/3TC drug combination was commonly used with other classes of drugs from mid-1990s to early-2000s. Currently, newer NRTI combinations like Kivexa (abacavir (ABC) and lamivudine) or tenofovir/emtricitabine are used in cART, as regimens with AZT required more frequent doses, have a higher risk of resistance mutations and are associated with toxic side effects like lipoatrophy and anemia.[18]

1.2.2 The Effects of cART Exposure on Genomic Stability:

While the effectiveness of cART, particularly in reducing the risk of vertical HIV transmission, is well-established, there are serious concerns about its side effects.[23,24] The effects of NRTI exposure on mitochondrial health have been examined extensively, with children exposed to AZT/3TC *in utero* experiencing mitochondrial toxicity, low mitochondrial DNA content and mitochondrial morphological damage.[25] Other effects include mitochondrial DNA depletion in AZT-treated people living with HIV as well as reduced mitochondrial DNA replication in *in vitro* studies.[26,27]

Conversely, concerns about the effects of NRTI exposure on nuclear DNA are not as well-studied. AZT in particular has been the focus of many genotoxic studies, with one study reporting DNA lesions and mutations in reporter genes indicating somatic recombination or gene conversion events.[28] Other studies assessing the prenatal effects of AZT have reported oxidative DNA damage and high micronuclei frequency, indicating chromosomal DNA damage.[29,30] Studies assessing synergistic effects of the dual-NRTI treatment AZT with 2',3'-dideoxyinosine (ddI) have reported an increase in mutagenicity after exposure due to point mutations and complete gene deletions.[31,32] Increase in chromosomal DNA damage frequency after 24-hours of dual-NRTI (tenofovir disoproxil fumarate (TDF) and 3TC) and dual-NRTI plus NNRTI (AZT/3TC plus efavirenz (EFV)) exposure has also been observed.[33] One study has reported *in vitro* dose-dependent increases in mutation frequencies after single NRTI (AZT, 3TC, ABC) and dual-NRTI treatments (AZT/3TC). Among the single NRTI treatments, the mutation frequency after 3TC exposure was significant at a higher exposure concentration than the other single-NRTI treatments. In comparison with the single NRTI treatments, the AZT/3TC treatment was associated with a higher mutation frequency. The same study also exposed pregnant mice to AZT, 3TC and AZT/3TC drug

regimens and found an increase in a reporter gene mutation frequency in the AZT and AZT/3TC exposed pups on day 13 post-partum.[34]

These studies suggest that the genotoxic effects of NRTIs in cART may increase the risk of cancer in people living with HIV. AZT in particular is considered a carcinogen in adult mice, and prenatal exposure has been linked to high tumor formation in pups.[35,36] In humans, prenatal exposure to other NRTIs like didanosine has been associated with high cancer incidence.[37] Other studies assessing cancer risk in people exposed to NRTIs *in utero* have not found a greater risk after NRTI exposure, although these studies are limited in size, assessment period and drug regimen combinations.[38,39] Hence, more studies are needed to determine cART's genotoxicity and associated risks on genomic stability.

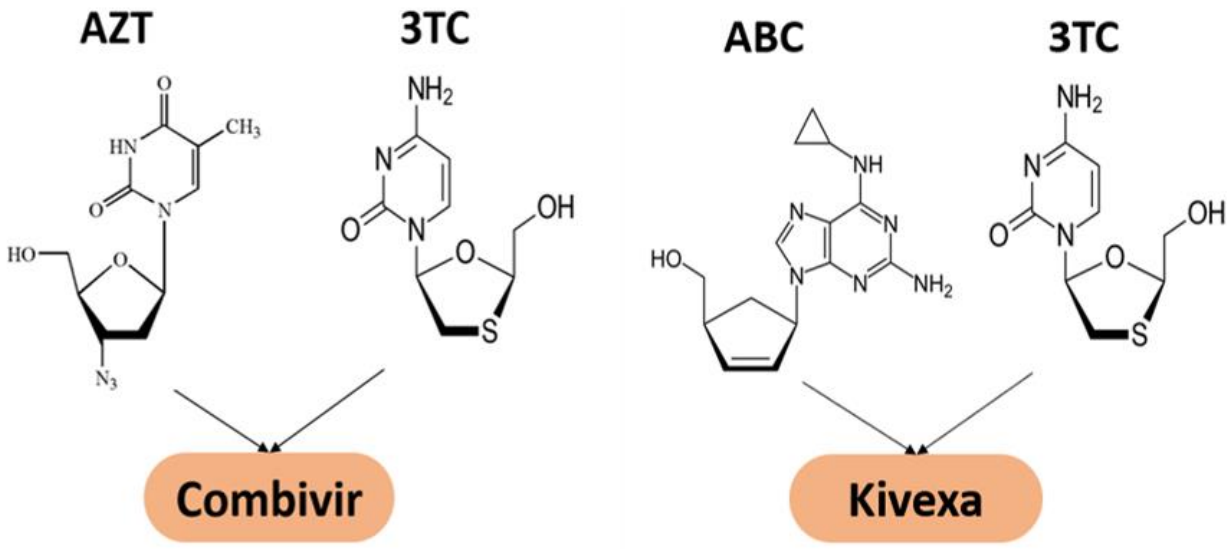

Figure 1. Anti-HIV NRTI combinations. Combivir is comprised of the NRTIs AZT and 3TC while Kivexa is composed of ABC and 3TC.

1.3 Pregnant Women Living with HIV:

Women are particularly at risk for HIV infection due to gender-based social and structural barriers.[40,41] With over 19 million adolescent girls and women living with HIV, research that considers the biological implications of sex is necessary for HIV prevention and control.[40] In Canada, approximately 80% of women living with HIV fall within the reproductive age.[42] Moreover, women of reproductive age living with HIV demonstrate a strong desire and intent to get pregnant. [42-43]

Current treatment guidelines set by the World Health Organization (WHO) as well as Canadian national recommendations emphasize the importance of taking cART for the mother's health and to prevent vertical transmission.[44,45] Earlier treatment guidelines concerning pregnant women living with HIV recommended various timings for initiating antiretroviral therapy.[46,47] Since 2015, WHO has modified these guidelines that now recommend immediate initiation and strict adherence of cART upon HIV diagnosis.[48] Consequently, developing fetuses are more likely to be exposed to cART from conception. Additionally, community-based efforts in resource constrained settings and public health initiatives based on these guidelines have facilitated easier access to cART.

1.3.1 cART and Changes in Pregnancy:

Although cART regimens are recommended for pregnant women living with HIV, the safety and toxicity information regarding their *in-utero* effects are limited. NRTIs can diffuse through the placenta and are found in umbilical cord blood, as well as the amniotic fluid.[49] In a successful pregnancy, fetal rejection by the mother's immune system is avoided by downregulating T-helper (TH) 1 cells to shift towards a TH-2 cell mediated immune response.[50] The shift towards

upregulating TH-2 cells is also observed in untreated people living with HIV who are in the early stages of the HIV infection. Exposure to antiretroviral treatment resulted in changes in the cytokine profile, indicating immune reconstitution through a shift back towards the TH-1immune response.[51] TH-1 cells produce cytokines such as interleukin (IL)-2 which compromise pregnancy. IL-10 is a regulatory cytokine product of TH-2 cells that is associated with a successful pregnancy. High IL-2 and low IL-10 levels have been reported in pregnant women living with HIV and taking three or more antiretroviral drugs. These cytokine levels have also been associated with premature delivery.[52]

Current studies have linked adverse birth outcomes like stillbirths, preterm delivery and smaller for gestational age with exposure to anti-HIV drugs *in utero*.[53] Adverse birth outcomes, specifically fetal growth restriction, have been linked to a disruption in placenta vascular development and remodeling as well as lower progesterone levels, which in turn may be caused by low prolactin and high progesterone-regulating enzyme 20-α-hydroxysteroid dehydrogenase levels.[54–56] Other studies have reported altered estradiol levels in pregnant women living with HIV and adhering to cART regimens, with higher and lower levels observed differentially depending on PI-based or NNRTI-based cART. Both higher and lower estradiol levels were associated with a higher risk of children who are small for gestational age.[57,58] These dysregulations could impact pregnancy outcomes, disrupt sex-specific differentiation of fetal gonads, and affect epigenetic modifications like DNA methylation during the gestation period which in turn could impair the sexual differentiation process while also potentially damaging testicular and ovarian structure.[59]

1.3.2 Fertility Associated Complications of cART Use in People with HIV:

The effects of antiretroviral therapy on fertility in adults living with HIV have been explored. Lower mitochondrial DNA levels in sperm, poor spermatozoa motility, decline in semen volume, abnormal sperm morphology and a reduction in total sperm count has been reported for men living with HIV and taking at least two anti-HIV drugs.[60–62] Using atomic force microscopy, a 2004 study analyzed spermatozoa morphology and topography in men living with HIV and taking antiretroviral therapy versus men living with HIV who had never taken antiretroviral drugs. The study concluded that spermatozoa damage was due to antiretroviral drug exposure, and not the result of the HIV virus itself.[63] The impact of antiretroviral drugs on the fertility of female adults is more complex. In adult women living with HIV, low mitochondrial DNA levels in oocytes, a dysfunction typically associated with infertility, has been reported.[64] However, antiretroviral drugs are also credited with reducing the fertility gap between healthy women and women living with HIV, and are associated with higher pregnancy rates.[65–68] Although existing studies have increased our understanding of the effects of cART on adults and on immediate clinical events like birth outcomes, a significant knowledge gap exists about the long-term reproductive health of children exposed to current and newer NRTI combinations *in utero*.

1.4 DNA Methylation

The study of epigenetics examines genome transformations that are heritable and reversible but are not caused by changes in the DNA sequence. DNA methylation is a specific type of epigenetic modification that regulates gene expression. Genetic sequences can include CpG islands, which are regions with high concentrations of cytosine (C) and guanine (G) dinucleotides. A phosphate (p) bond joins the nucleotides.[69] DNA methylation changes the function of genetic

sequences by covalently attaching a methyl group to the cytosine of a CpG dinucleotide. The cytosine now becomes 5-methyl cytosine. DNA methylation is carried out by DNA methyltransferases (Dnmts). CpG islands include large clusters of unmethylated CpG dinucleotides. Depending on their methylation status, CpG islands in a gene's promoter region control gene expression. DNA methylation is largely linked to gene silencing. The addition of methyl groups limits access to the promoter, which in turn inhibits the binding of transcription factors and leads to gene repression.[69]

1.4.1 DNA Methylation, Embryo Development and Reproductive Capacity

A zygote is created from the fertilization event between male gametes (sperm) and female gametes (oocyte). After several rounds of mitosis, a blastocyst is formed. A blastocyst has an inner cell mass, and a fluid filled cavity which is enclosed by trophectoderm cells.[70,71] After the blastocyst is embedded into the wall of the uterus, gastrulation begins where the embryo differentiates into germ cells and into the three germ layers that give rise to somatic cells. The primordial germ cells increase in population and move towards the genital ridge, which eventually forms the gonads.[70] As primordial germ cells proliferate and migrate, their pre-existing DNA methylation patterns disappear globally in a process known as *de novo* DNA methylation.[70]

After sexual differentiation, sex-specific germ cell DNA methylation patterns are formed. For the male embryo, DNA methylation patterns re-appear in pro-spermatogonia, which are mitotically arrested in the G1-phase. DNA methylation patterns are fully established by birth. The mitotic arrest before birth in males is followed by mitotic proliferation after birth and then meiosis occurs at the onset of puberty. For the female embryo, meiosis begins before birth, with the primary oocyte being arrested in the first meiotic prophase. DNA methylation patterns are only formed

after birth in growing oocytes. At the onset of puberty, the release of luteinizing hormone completes prophase I of meiosis I in the developed oocytes. The release of the first polar body is followed by the second meiotic arrest and fertilization.[70]

After fertilization, epigenetic reprogramming including DNA demethylation of the genome depends on the parental origin of the genome. While an active demethylation mechanism rapidly removes the DNA methylation marks from the paternally contributed genome, the DNA methylation pattern of the maternally contributed genome gradually declines throughout a process called passive demethylation.[70] Genomic imprinting of genes is an epigenetic process where depending on the parental origin, only one copy of the gene is active. Maternally imprinted genes have an active paternally inherited allele and a silent maternally inherited allele. Paternally imprinted genes have an active maternally inherited allele and a silent paternally inherited allele. Many imprinted genes display differentially methylated regions.[70,72] Imprinted germline differentially methylated regions do not undergo demethylation after fertilization. Imprinted gene expression depends on maintaining the parental allele-specific DNA methylation marks, hence differentially methylated regions are imprinting control regions.[70]

Adverse environmental exposure during the early stages of embryogenesis can change epigenetic processes like DNA methylation. This can alter imprinted gene expression which can affect fetal and placental growth.[73] Existing studies have linked abnormal methylation patterns of imprinted genes to stillbirths, spontaneous pregnancy losses, reduced male fertility and pathologies of reproductive organs like the uterus.[74–76] Hence, DNA methylation patterns of imprinted genes have an important role in reproductive health and regulating fertility.

1.5 Germ Cell Development and Differentiation:

Meiosis is a highly regulated and conserved process. Using a two-step specialized cell division pathway, the ultimate goal of meiosis is to create daughter cells, also known as gametes, with a haploid genome. The first meiotic division (Meiosis I) includes the pairing and subsequent segregation of homologous chromosomes.[77] Nondisjunction occurs if the paired homologous chromosomes do not successfully separate.[78] It can lead to aneuploidy, a genetic condition where a cell has an irregular number of chromosomes. Interestingly, with frequencies as high as 10-30%, aneuploidy is unusually common in humans. Clinically, aneuploidy can cause loss of pregnancy and developmental abnormalities in the child.[78]

In prophase I, the first step of meiosis I, the duplicated homologous chromosomes condense and create tetrads. This chromosomal configuration facilitates the creation of new gene combinations through crossing-over, where the chromosomes exchange genetic information. During metaphase I, the tetrads line up in the middle of the cell and in anaphase I, the contraction of the spindle fibers separate the homologous pairs of chromosomes to opposite sides of the cell. In telophase I, the reformation of the nuclear membrane encloses the chromosomes. The cell undergoes cytokinesis by splitting its cytoplasm to give rise to two haploid daughter cells.[79]

The second meiotic division (Meiosis II) is comparable to mitosis, as it involves the separation of sister chromatids. Prophase II includes the condensing of chromosomes and the creation of spindle fibers. In metaphase II, the sister chromatids line up at the metaphase plate. The sister chromatids are then detached at the centromeres and moved to opposite ends of the cell in anaphase II. Each sister chromatid is now considered a separate chromosome. Like telophase I, telophase II entails the reformation of the nuclear membrane and cytokinesis. Completion of both meiotic divisions gives four haploid daughter cells.[79]

1.5.1 Sexual Development:

Many attributes of meiosis like initiation, duration and final result vary by sex. Meiosis only occurs in germ cells, which are located in the gonads. Male gonads are testes and female gonads are ovaries.[78] During fetal testes development, mitotic arrest follows a short-lived period of mitotic proliferation before continuing mitotic arrest. This mitotic arrest lasts until birth. After birth, mitotic proliferation begins again. Meiosis in male germ cells, also known as spermatogonia, only occurs after the initiation of puberty. Following meiotic entry, male germ cells continuously undergo mitotic and meiotic divisions to generate sperm (haploid gametes) throughout the male lifespan.[78]

Spermatogenesis is the process that describes male germ cell differentiation and growth.[80] It occurs in the seminiferous tubules. Immature spermatogonia complete mitosis and give rise to type A spermatogonia, which contribute to the seminiferous tubules' epithelium, and type B spermatogonia, which mature into primary spermatocytes. Following the first meiotic division, the primary spermatocytes give rise to secondary spermatocytes, which complete the second meiotic division to produce spermatids. Through the maturation process of spermiogenesis, spermatids undergo morphological changes and are converted to spermatozoa.[80]

Oogonia are female germ cells that stop mitotic proliferation and commence meiosis I in the fetal ovary. After entering meiosis, oogonia are known as oocytes. Before birth, oocytes are arrested in prophase I. At birth, somatic cells have encircled the developing primary oocytes to make primordial follicles.[78,81] Upon reaching sexual maturity, female reproductive hormones regulate the menstrual cycle, which includes a follicular phase, ovulation and a luteal phase.[81]

The process of folliculogenesis describes the growth stages of ovarian follicles. Since the development of primordial follicles and the start of meiosis occurs during gestation, new oocytes

cannot be generated after birth. Primordial follicles are considered “non-growing” follicles and undergo a regular recruitment process for growth.[82] Recruited primordial follicles then enter the pre-antral growth phase, which includes the primary and secondary follicle developmental stages.[82,83] Once the fluid in the secondary follicles accumulates into a cavity called an antrum, the follicles reaches the tertiary developmental stage and are now known as antral follicles. The oocyte in the antral follicle has completed structural development. From these follicles, a dominant follicle is selected for ovulation through an unknown mechanism while the remaining follicles and their oocytes breakdown and undergo atresia, also known as follicular apoptosis.[78,82] Just before ovulation, a luteinizing hormone (LH) surge occurs. This completes meiosis I and the female germ cells, now called secondary oocytes arrest in metaphase of meiosis II.[81] The ovulated mature female germ cell called the ovum completes meiosis II after fertilization. In the luteal phase, the ruptured follicles develop into an endocrine organ called the corpus luteum, which is degenerated through apoptosis in the absence of fertilization.[81,82,84]

1.5.2 HIV Antiretrovirals and their Impact on Reproductive Capacity

Incorporation of anti-HIV drugs into DNA can affect genetic and chromosomal integrity.[85] Existing studies examining the genotoxicity of anti-HIV drug exposure have observed the formation of micronuclei, which are created from improper chromosome segregation during anaphase in mitotic or meiotic division.[85,86] Micronuclei are associated with pregnancy complications like miscarriages and reduced reproductive potential like DNA damage in sperm. Not only are micronuclei present in higher concentrations among couples with damaged reproductive capacity, but their frequency also correlates with abnormal sperm morphology.[86]

Other harmful effects include the shortening of telomere lengths.[85] Telomeres are repetitive DNA sequences that prevent damage to the ends of chromosomes. During meiosis, telomeres have

an important role in the creation of the chiasmata and in managing homologous chromosome pairing.[87] Germ cell precursors express telomerase which protects telomere length. High telomerase activity is observed in early oogenesis to maximize telomere length.[87] Reduction in telomere length correlates with aneuploidy, reduced chiasmata formation and a higher incidence of apoptosis before embryo implantation. All these factors contribute to a lower reproductive capacity.[87]

1.5.3 Histopathology Parameters of Fertility

Several parameters like hormone levels and ovarian volume have been explored for their ability to predict reproductive potential in females. From these biomarkers, antral follicle number is considered the best reflection of reproductive age and is also associated with the number of primordial follicles available in the ovarian reserve.[88,89] For the purposes of histological identification, a primary follicle contains an oocyte surrounded by cuboidal granulosa cells organized in one layer.[82] The oocyte in a secondary follicle is surrounded by an extracellular matrix called the zone pellucida, which is encased by at least two cuboidal granulosa cells layers. The antral follicle has a structurally developed oocyte coated by the zona pellucida, a characteristic fluid-filled antrum and several cuboidal granulosa cells layers.[82] The corpus luteum is distinguishable for its missing oocyte. Although the histological appearance of the corpus luteum can vary depending on its developmental progress, the corpus luteum in mice may have a granulated appearance with vascular tissue and large cells.[90]

In males, the testes are packed with seminiferous tubules, which are the site of spermatogenesis.[80] In current literature, a histological assessment of testes includes examining the diameter of seminiferous tubules, with smaller diameters being indicative of a low fertility

potential due to complications like fewer germ cell numbers and/or loss of seminiferous tubule fluid.[91–93] Other assessments involve quantifying Sertoli and Leydig cell numbers.[91,94–96] Leydig cells are in the interstitial space surrounding seminiferous tubules and make testosterone, a sex steroid hormone.[97] Leydig cells have a polyhedral shape and can be found in clusters.[80] Sertoli cells are located with developing germ cells inside the seminiferous tubules. They are arranged from the tubule wall to the tubule lumen. Sertoli cell functions include facilitating spermatogenesis by ensuring germ cells have access to growth factors, nutrients and a healthy niche.[97] Sertoli cells are tall with a columnar shape and oval nuclei.[80] Their activation depends on the follicle-stimulating hormone (FSH). Sertoli cells secrete seminiferous tubule fluid which contributes to lumen formation, androgen-binding protein (ABP) which accumulates testosterone within the seminiferous tubule and inhibin which prevents FSH secretion.[80,97]

Attached to the testis' surface, the epididymis links the testis to the vas deferens, another organ in the male reproductive system.[98] The epididymis has many functions which greatly contribute to male fertility potential. Once spermatozoa enter the epididymis from the testis, sperm maturation begins. After maturation, sperm are stored in the epididymis until ejaculation. Estrogen and androgens like testosterone can regulate gene expression in the epididymis.[98] A decline or loss in androgen levels adversely affects spermatozoa's ability to move, fertilize and survive.[99] Studies examining fertility have used various histopathological markers to characterize the effects of external agents and mutations on epididymal health. These markers include the degeneration of epithelial cells and the presence of vacuoles in the epithelial cell layer of the epididymal ducts.[100,101] Other markers are the identification of hyperplasia and sperm granuloma.[101] Sperm granuloma are formed by immune cells, white blood cells and granulation tissue which all cluster around mature spermatozoa released from damaged epididymal ducts. Some of the spermatozoa

in this mass may begin degradation, hence reducing the number of available mature sperm.[102] All of these histopathological markers have been associated with reduced fertility.

2.0 RESEARCH OBJECTIVE & AIMS

The emergence of cART has transformed the HIV diagnosis from a death sentence to a more manageable condition. However, while cART's near elimination of HIV vertical transmission is a public health success story, there are increasing concerns about the genotoxic effects of *in utero* cART exposure on the health of HIV exposed but uninfected children.[25, 85, 103, 104] These concerns are particularly pressing given that women living with HIV have a strong intent to get pregnant and have improved access to cART.[3,42,43] Moreover, due to updated treatment guidelines, HIV exposed children are now also exposed to cART right from conception and throughout the pregnancy.[44,45,48] Given that primordial germ cell development starts before birth, early exposure to anti-HIV drugs could not only affect the fertility of children exposed *in utero*, but could also have lasting implications on the reproductive health of future generations.

The Serghides lab has used a mouse pregnancy model to examine placenta vascular changes and progesterone levels after exposure to cART regimens.[54,55] The Sabatinos lab has used a fission yeast model to show that NRTI-exposure increases the DNA mutation rate (Su, C. In Preparation, Ryerson University 2018). Using the expertise of both lab groups, we will investigate the effects of *in utero* NRTI- and cART-exposure on genomic stability and germ cell development. Our ultimate goal is to improve our understanding of *in-utero* cART exposure on the reproductive health of offspring.

<u>Aim I: What are the effects of nucleoside analogs on genome stability?</u>

Rationale: Due to its integration within nuclear and mitochondrial DNA, AZT, a NRTI used in some cART regimens, has been linked to genome instability.[104,85] While the effects of AZT monotherapy are well-studied, AZT's effects in conjunction with 3TC as well as the effects of

newer anti-HIV drugs on the genome are unknown. Characterizing the effect on genome stability is important because DNA mutations, cellular toxicity and epigenetic dysregulation like aberrant DNA methylation patterns can affect the expression of genes necessary for fetal growth and reproductive health. Hence, to determine the effects of nucleoside analogs on genome stability, we will calculate the DNA mutation rate and assess cellular toxicity. Our next step will then examine changes in DNA methylation patterns after NRTI exposure.

Methods: A fission yeast mutation rate assay previously established for other nucleoside analogs will be used to determine the mutation rate. The web tool FALCOR will be used to calculate the mutation rate.[105] Cellular toxicity will be assessed using Trypan Blue. Bisulfite-sequencing will be used in the future to assess the DNA methylation patterns of mouse sperm collected from mice exposed to anti-HIV drugs *in utero*.

Hypothesis: Prolonged exposure to combination NRTIs will be associated with increased DNA mutations and high cellular toxicity, thus indicating reduced reproductive potential and poor fertility.

Aim II: What are the effects of nucleoside analogs on germ cell development?

Rationale: The genotoxic effects of anti-HIV drugs give rise to micronuclei and shorten telomere lengths; both effects may disrupt meiotic division and lower reproductive capacity.[85–87] Given that primordial germ cell development, meiotic initiation in females, and preparation for meiotic initiation in males occur before birth, exposure to anti-HIV drugs *in utero* could have adverse consequences for later fertility.[77–79] Hence, to determine the effects of anti-HIV drug exposure *in utero* on the offspring's reproductive health, we will assess ovarian follicles and testis structure to examine the impact on germ cell development.

Methods: An immunohistochemical analysis will be conducted using the slides with paraffin sections of mice testes and ovaries. These samples will be collected from mice exposed to anti-HIV drugs *in utero*.

Hypothesis: In-utero exposure to anti-HIV drugs will be associated with low ovarian follicle numbers and disrupted testis structure, thus indicating reduced reproductive potential and poor reproductive health.

3.0 MATERIALS AND METHODS

3.1 Fission Yeast:

Schizosaccharomyces pombe, also known as fission yeast, is a well-established model organism for cell biology and genetic research.[106] As a rod-shaped unicellular eukaryote, *S. pombe* is 4 µm wide and measures 7-14 µm in length at various points in the cell cycle.[106,107] In contrast to the more common brewing yeast *Saccharomyces cereviseae* counterparts, specific molecular and genetic mechanisms of *S. pombe* are highly comparable to mammals.[108] *S. pombe*'s chromosomal structure, including telomeres and origins of replication, parallel that of mammals.[106,109] Moreover, fission yeast responds to nucleoside analogue drugs at comparable concentrations to human cells.[105] Hence, fission yeast is an excellent model organism for testing genome stability in response to nucleoside analogue drug exposure.

All fission yeast strains are genetically engineered with transgenes: the Herpes Simplex Virus thymidine kinase (*hsv-tk*$^+$), and the human equilibrative nucleoside transporter 1 (*hENT1*$^+$) (Table 1). These transgenes allow for uptake (*hENT1*$^+$) and use (*hsv-tk*$^+$) of nucleoside analog drugs.

Table 1. The genotype of the fission yeast strains.

Strain	Genotype
Incorporating wild type (*wt*) FY2317	*h+ leu1-32::hENT1-leu1+(pJAH29) his7366::hsv-tk-his7+(pJAH31) ura4-D18 ade6-M210*
Incorporating *mrc1*Δ FY3179	*h+ mrc1Δ::ura4+ leu1-32::hENT1-leu1+(pJAH29) his7-366::hsv- tk-his7+(pJAH31) ura4-D18 ade6-M210*
Incorporating *cds1Δ* mutant FY5148	*h+ cds1Δ::ura4 leu1-32::hENT1-leu1+(pJAH29) his7-366::hsv-tk- his7+(pJAH31) ura4-D18 ade6-M210*
Incorporating *chk1Δ* mutant FY5149	*h+ chk1Δ::ura4+ leu1-32::hENT1leu1+(pJAH29) his7-366::hsv- tkhis7+(pJAH31) ura4-D18 ade-704*
Incorporating *rad3Δ* mutant FY5150	*h+ rad3Δ::ura4+ leu1-32::hENT1leu1+(pJAH29) his7-366::hsv- tkhis7+(pJAH31) ura4-D18 ade6-M210*

These fission yeast strains were gifted by Dr. Susan Forsburg from the University of Southern California, USA.

3.1.1 Fission Yeast Cell Cycle Checkpoints:

Progression through the cell cycle is controlled by cell cycle checkpoints (Figure 2). Upon exposure to stress or damage, checkpoints prevent entry into the next cell cycle phase.[110] Fission yeast's DNA replication checkpoint stops cell-cycle progression using S-phase checkpoint proteins (Figure 3). DNA replication stress such as replication fork stalling causes Rad3-activation, and recruitment and phosphorylation of Cds1. A mediator protein Mrc1 is involved in Cds1 recruitment. The replication checkpoint prevents fission yeast cells from entering M-phase.[111,112] DNA double stranded breaks (DSBs) can be caused by various factors including drugs, radiation and other stress-inducing agents.[110] DSBs activate the DNA damage checkpoint response through Rad3-dependent phosphorylation of Chk1 via the mediator protein Crb2 (Figure 3). Once activated, the checkpoint arrests the cell cycle and prevents cells from advancing to M-phase.[113,114]

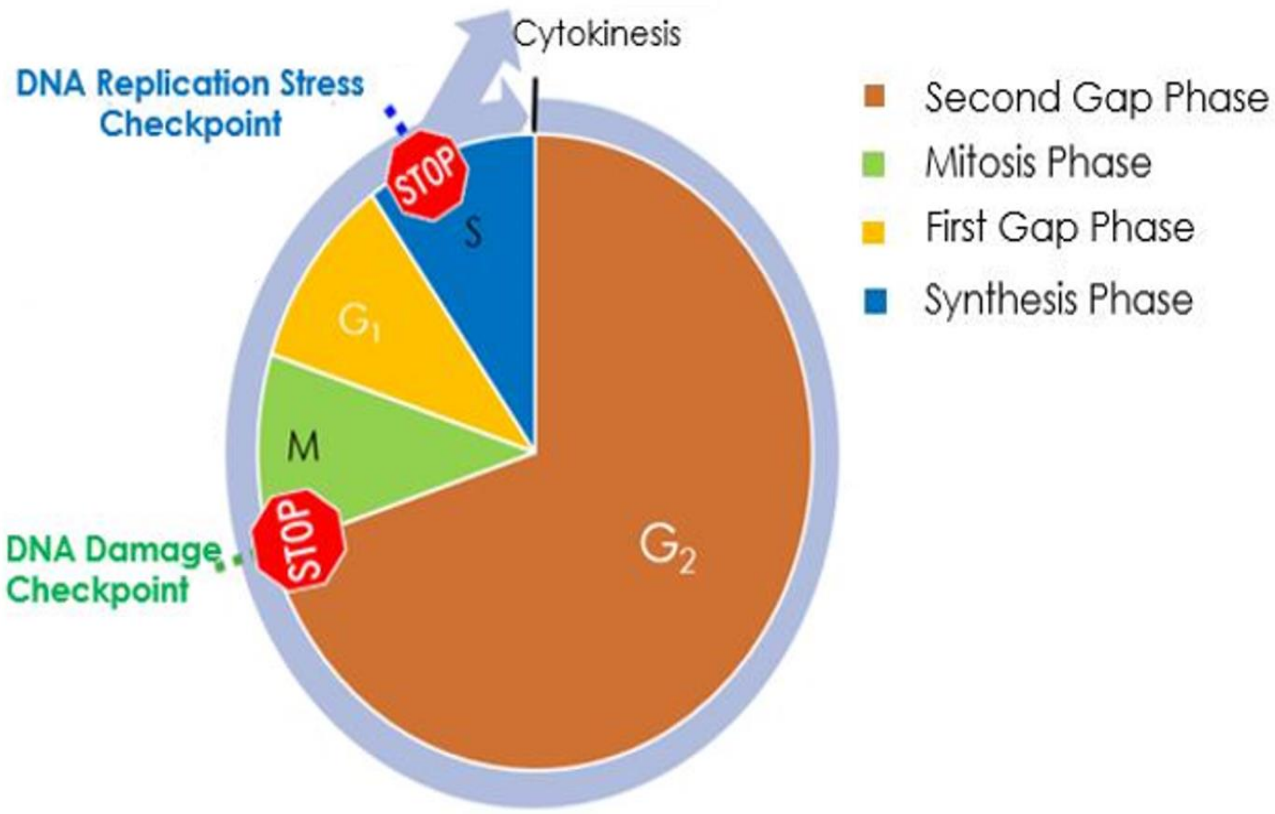

Figure 2. The fission yeast cell cycle. The four cell cycle stages are G_2, M, G_1 and S-phases. Fission yeast cells spend 70% of the cell cycle in G_2. The remaining 30% of time spent in the cell cycle is divided equally among the other three phases.

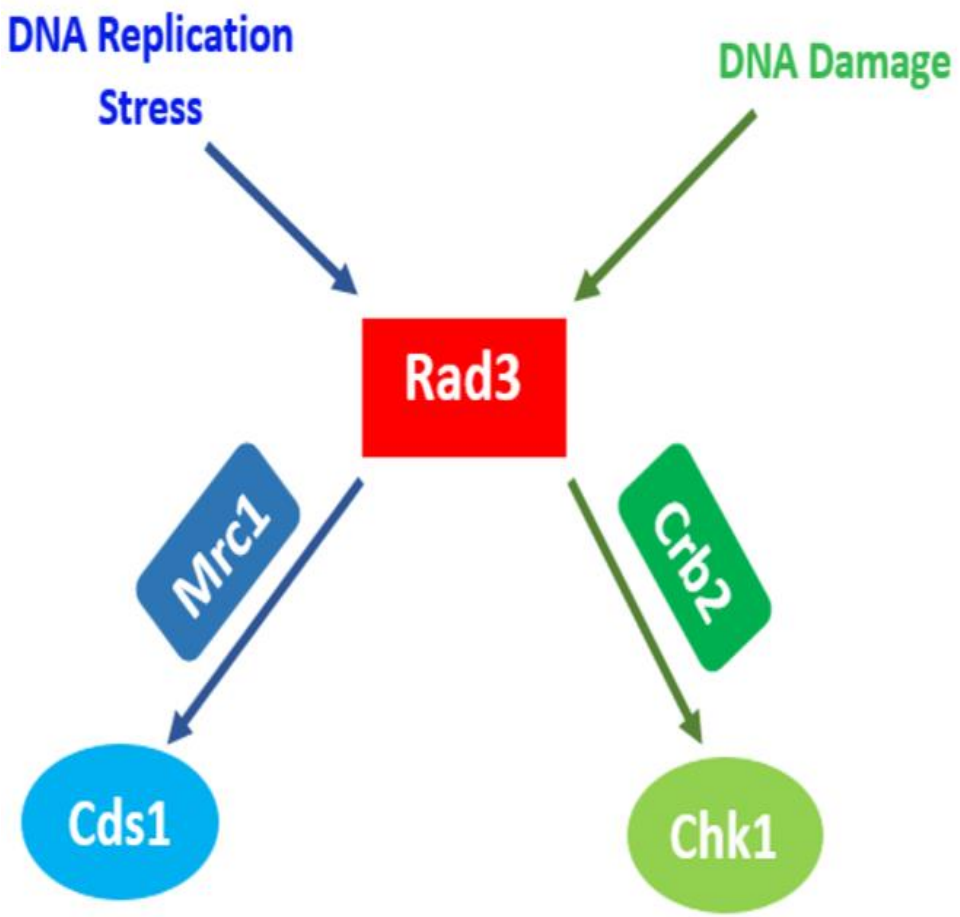

Figure 3. Fission yeast checkpoint protein pathways for DNA replication stress and damage. Both checkpoint pathways are mediated through Rad3-dependent phosphorylation.

3.2 Canavanine Mutation Rate Assay in PMG-UA with Trypan Blue:

Overnight cultures of all fission yeast strains were made in Pombe Glutamate Media (PMG) (Sunrise Science Products, California, USA) supplemented with Uracil (U) and Adenine (A). Hereafter, we will refer to this media as incomplete media as it is missing Histidine (H) and Leucine (L). The optical density for each strain was recorded using a spectrophotometer set at a wavelength of 600 nm. After incubating 2 mL of the overnight cultures in a shaking water bath for 1 hour, AZT (1 mM) and 3TC (150 µg/mL) was added to each sample to create the 0-hour timepoint. From each culture, 500 µL was transferred to Eppendorf tubes, from which 450 µL was plated on canavanine plates. Canavanine plates were made by mixing stock canavanine (70 µg/mL) in PMG-UA with Phloxine B. An aliquot of 20 µL from each culture was serially diluted in 180 µL of Yeast Extract with Supplement (YES). The 10^3 dilution was plated on two YES plates. All plates were incubated at 30°C for colony growth.

An aliquot from each culture was mixed with Trypan Blue in a 1:1 ratio and incubated at room temperature for 30 minutes. With light microscopy, a hemocytometer was used to count the stained and unstained cells for each strain

YES plates were scored after 3 days while canavanine plates were scored after 11 days. The mutation frequency was calculated by dividing the number of colonies growing on canavanine plates with the total number of cells plated. The mutation rate was calculated using the web tool known as Fluctuation Analysis Calculator (FALCOR). All steps were repeated for 6- and 24-hour timepoints (Figure 4).

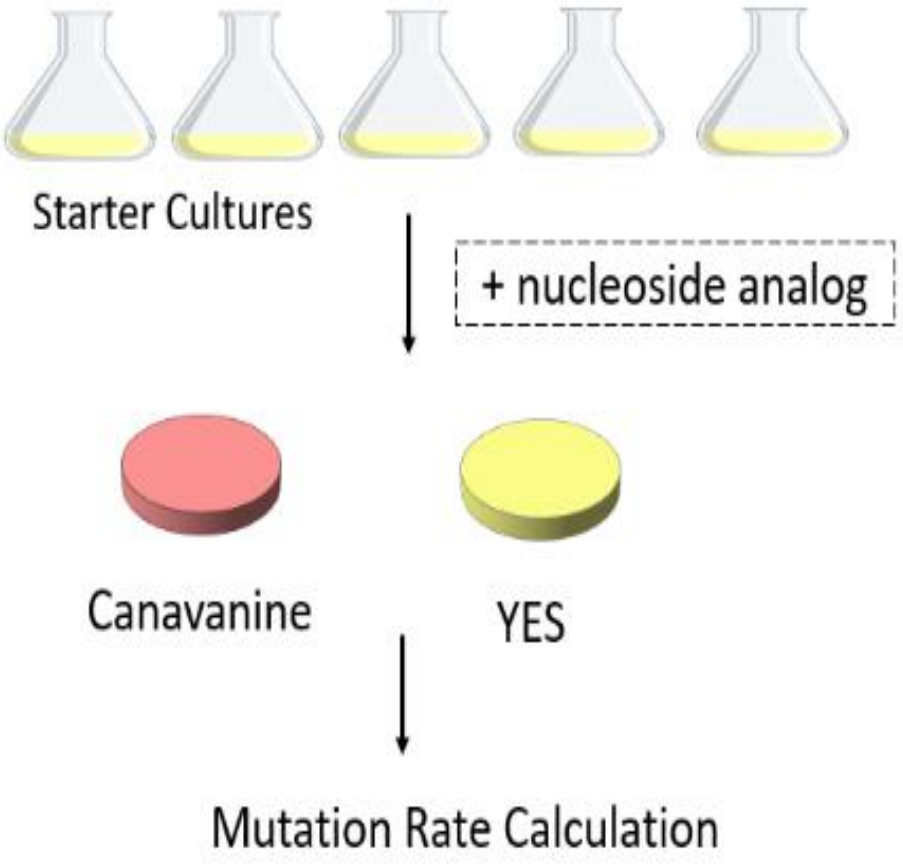

Figure 4. Schematic diagram of canavanine mutation rate assay. This assay looks for the loss of *Can1* function in *S. pombe,* which leads to colony formation on canavanine plates. By comparing colony growth to Yeast Extract with Supplement (YES) titre plates, the mutation rate can be calculated using the web tool FALCOR.

3.3 Canavanine Mutation Rate Assay in PMG-HULA with Trypan Blue:

All steps from Canavanine Mutation Rate Assay in PMG-UA with Trypan Blue were followed with two major exceptions. The canavanine plates were made from PMG-HULA (Pombe Glutamate Media supplemented with Histidine, Uracil, Leucine and Adenine) as opposed to PMG-UA media. Hereafter, we will refer to this media as complete media as it is includes Histidine (H) and Leucine (L) and hence is considered complete media. The 10^3 dilution of overnight cultures with drug were also plated on two YES plates for the 0- and 6-hour timepoint but the 10^4 dilution was used for the 24-hour timepoint. The experimental setup was modeled after existing mutation rate studies examining nucleoside analogs 5-bromo-2'-deoxyuridine (BrdU) and 5-ethynyl-2'-deoxyuridine (EdU).[105]

3.4 Mouse Pregnancy Model and Drug Administration:

C57BL/6 mice were purchased from the Jackson Laboratories. Before mating, females were trained for 7 days on oral gavage with water. This was done to reduce any potential stress oral gavage may cause on the pregnancy. Female mice were group housed as 4 dams per cage. Males were single housed for 7 days prior to mating. Sexually mature female mice aged 8-10 weeks old were mated with males. Mating was confirmed the next morning based on the existence of vaginal plugs (designated gestational day (GD) 1). While vaginal plugs suggest copulation, they do not confirm pregnancy. To verify pregnancy, dams were weighed on gestational day 9 (GD9) and gestational day 13 (GD13). Pregnancy was confirmed if the female mice weighed more than 1.5 g on GD9 and more than 3 g on GD13.

C57BL/6 mice were divided into a control and treatment group. Using oral gavage, the mice in the control group were given water while the treated group received 100/50 mg/kg/day of

ABC/3TC with 50 mg/kg/day of the protease inhibitor ritonavir-boosted atazanavir (ATV/r). The anti-HIV drug dosages reflect the optimal dosage necessary to achieve plasma concentrations equivalent to those seen in pregnant women. All treatments were administered daily starting from GD1 until delivery.

F1 male and female pups were weaned at postnatal day (PND) 21. After PND21, the pups were separated by sex and housed until sexual maturation (PND49) was achieved. The F1 generation was euthanized at 8-weeks. The gonads were dissected and weighed. Sperm were collected from the epididymis for DNA methylation analysis.

3.5 Tissue Preparation and Sectioning:

Mice testes and ovaries were fixed in formalin and embedded in paraffin wax. The microtome was set to create 5 µm tissue sections. The paraffin sections were placed on slides and stored at room temperature.

3.6 Hematoxylin and Eosin (H&E) Staining:

Slides with paraffin sections were soaked in Xylene to deparaffinize and then rehydrated in decreasing concentrations of ethanol. After immersing in water, the sections were stained in Gill's hematoxylin, washed with water and then dipped in acid alcohol to destain. Following another round of water, the sections were stained with eosin. The stained sections were dehydrated in increasing concentrations of ethanol and then submerged in Xylene. The slides were mounted using xylene based Permount. Using a Leica brightfield microscope with a Nikon camera attachment, images were recorded and observed on the NIS-Elements BR software.

3.7 Assessment of H&E Stained Ovarian Follicles:

Ovaries were quantified by counting the phases of folliculogenesis (Figure 5), while being blinded to the treatment allocation. Primary and secondary follicles were counted together as one group. Antral follicles and corpus luteum were respectively counted as separate groups. One 5 μm tissue section on one slide from each ovary was quantified. The proportion of follicles in each group was calculated by dividing the number of follicles in each specific group by the total number of follicles.

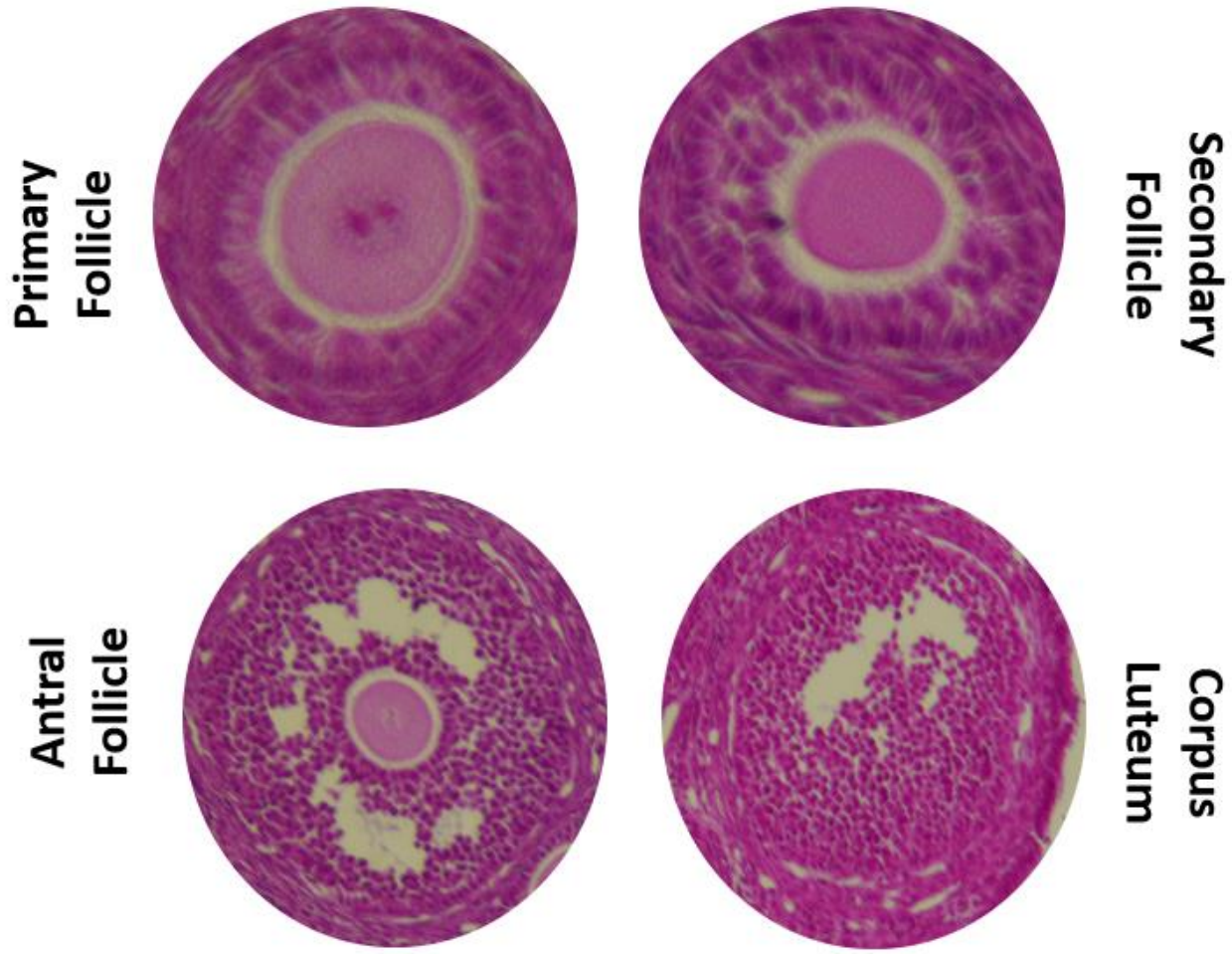

Figure 5. Stages of folliculogenesis. Primary follicles, secondary follicles, antral follicles and corpus luteum were scored, with primary and secondary follicles being grouped into one category. The histological parameters used identify each follicle stage are described in Section 1.6.3.

3.8 Assessment of H&E stained Testes:

All histometric testes assessments were conducted on one 5 µm tissue section on one slide from each testis. The assessor was blinded to the treatment allocation.

3.8.1 Diameter of Seminiferous Tubules:

The diameter of one seminiferous tubule was calculated at 10X magnification by finding the average of two diameter measurements. Both measurements were perpendicular to each other (Figure 6).[92] To obtain the average diameter of one section in a testis, the mean diameter of 20 seminiferous tubules was calculated.

3.8.2 Quantification of Sertoli and Leydig Cells:

All Sertoli and Leydig cells present in one field at 40X were counted (Figure 7). In one 5 µm tissue section, ten random fields were assessed. The total number of cells from the ten fields were plotted for each treatment allocation (Figure 15).

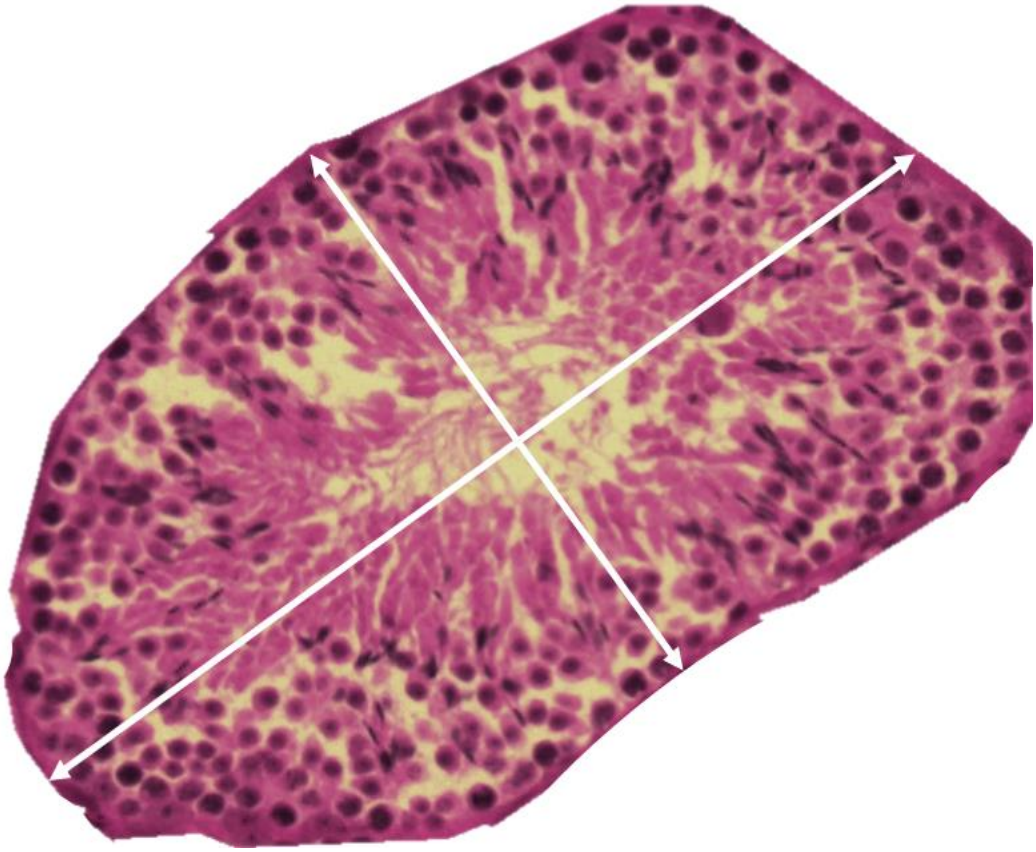

Figure 6. Diameter measurement of a seminiferous tubule. The diameter was calculated by taking the mean of two perpendicular diameter measurements (shown by white arrows) at a magnification of 10X.

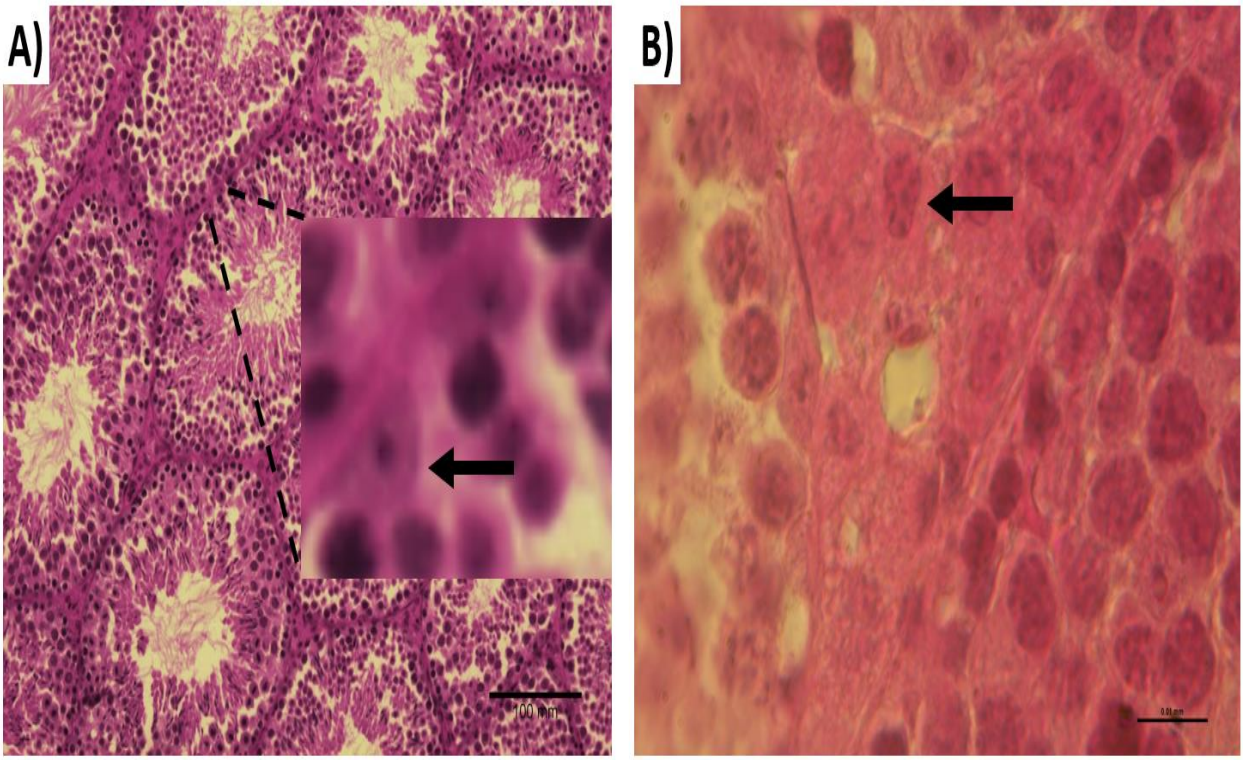

Figure 7. Identification of testis-specific cells that contribute to germ cell development. A) Sertoli cells (black arrow) were identified based on their characteristic tall, columnar shape and dark, oval nuclei. Scale Bar = 100 mm **B)** Leydig cells (black arrow) were found in the interstitial space between and around seminiferous tubules. Scale Bar = 0.01 mm.

3.9 Ethics Declarations:

All animal experiments were conducted following the Canadian Council on Animal Care guidelines and were approved by the University Health Network (UHN) Animal Use Committee.

3.10 Statistical Analyses:

All plots were created using GraphPad Prism version 8.0.[115] All statistical analyses were performed using VassarStats: Website for Statistical Computation.[116] A chi-square test and a two-tailed Mann-Whitney *U* test with significance levels of $\alpha = 0.05$ were used to compare the number of follicles at different stages. The two-tailed Mann-Whitney *U* test at $\alpha = 0.05$ was also used to assess the mean diameter of seminiferous tubules as well as the number of Sertoli and Leydig cells between the control and ABC/3TC with ATV/r treatment groups.

4.0 RESULTS

4.1 Effects of nucleoside analogs on genomic stability:

4.1.1 Canavanine Mutation Rate with complete media:

To determine the mutation rate of combined AZT/3TC exposure in complete media (PMG+HULA), the canavanine mutation rate assay was used with wildtype and cell cycle checkpoint fission yeast mutants (Figure 8). This is a well-established assay that has been previously used to test for the mutation rate of nucleoside analogs 5-bromo-2'-deoxyuridine (BrdU) and 5-ethynyl-2'-deoxyuridine (EdU).[105] In fission yeast, canavanine enters the cell through an arginine transporter coded by the *can1*$^{+}$ gene. Cells with the *can1*$^{+}$ gene cannot grow on canavanine. Exposure to mutagens can lead to *can1*$^{-}$ mutants, which can survive on canavanine as they are canavanine resistant.[105,117] Complete media is considered permissive media as it is supplemented with Histidine, Uracil, Leucine and Adenine and is the current standard media used to assess mutation rate in *S. pombe*. The fission yeast strains were plated on nutrient rich titre (YES) and canavanine plates after 0-, 6- and 24-hours of exposed to AZT/3TC drug treatment. Colonies growing on the YES plates were compared to the number of colonies growing on the canavanine plates. The mutation rate was calculated as the mean of 5 experimental replicates and plotted with upper and lower 95% confidence intervals (Figure 8). The mutation rate did not differ after 0- and 6-hours of drug exposure in all strains except *rad3Δ*, where the mutation rate increased after 6-hours of exposure. A large increase in mutation rate after 24-hours of combined AZT+3TC exposure also occurred in wildtype and all checkpoint mutants. This was indicated by the increase in colonies growing on canavanine plates, which was due to the loss of the *can1* gene function (*can1*$^{-}$).

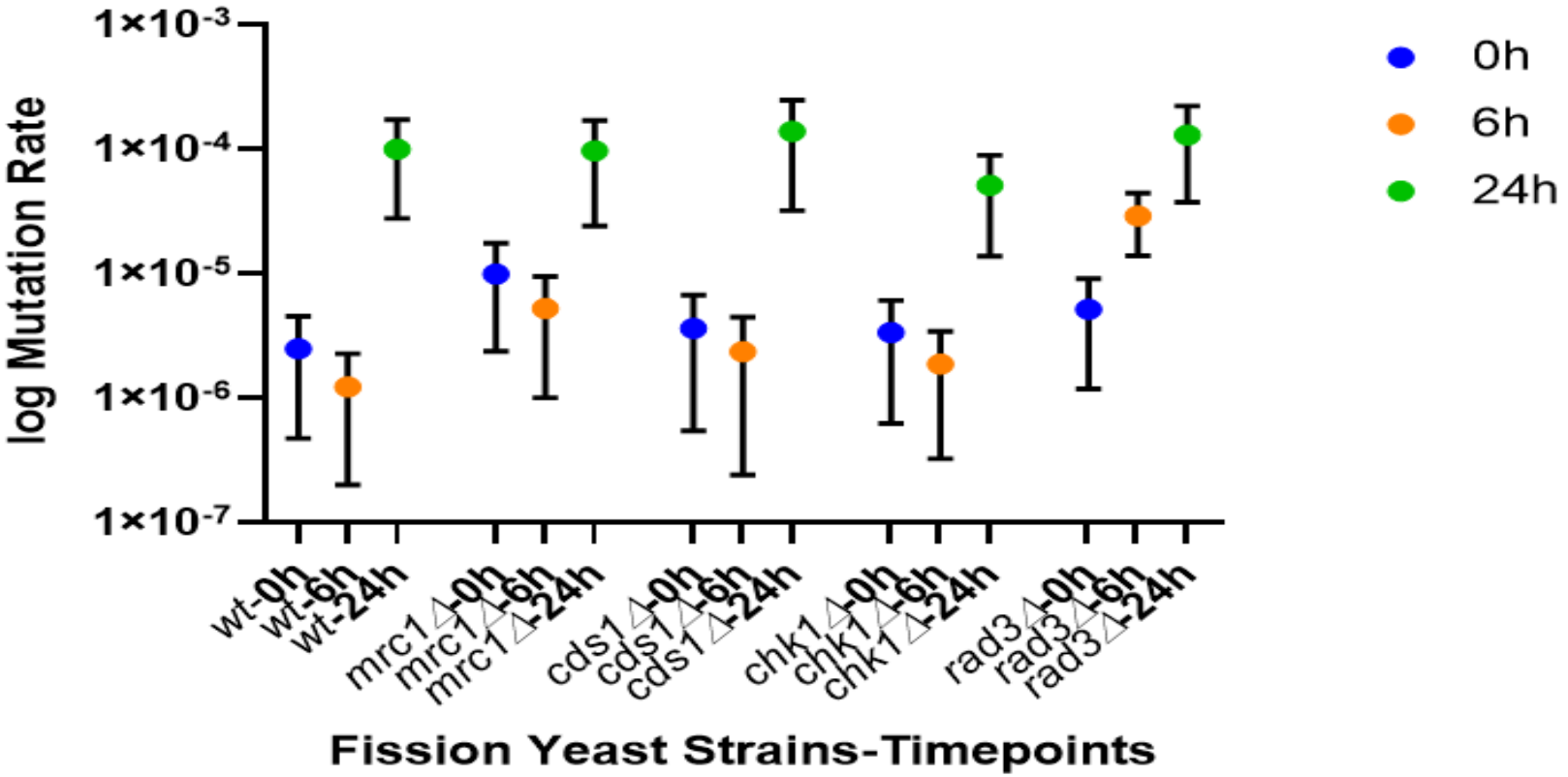

Figure 8. DNA mutation rate after AZT/3TC exposure with complete media. The mean DNA mutation rate was calculated over five experimental replicates by assessing the total number of wildtype and cell cycle checkpoint fission cells growing on YES plates with the *can1-* mutants growing on canavanine plates. The mutation rate after 6-hours of exposure increased in *rad3Δ* mutants and a greater rise in mutation rate was observed after 24-hours of exposure in all strains. Error bars indicate 95% confidence intervals (n = 5).

4.1.2 Canavanine Mutation Rate with incomplete media:

The mutation rate of combined AZT/3TC exposure in incomplete media (PMG+UA) was calculated using wildtype and cell cycle checkpoint fission yeast mutants (Figure 9). Incomplete media was only supplemented with Uracil and Adenine, thus creating conditions that would not allow growth of strains that had lost either the $his7^{+}$ or $leu1^{+}$ markers. Note that these markers are associated with the hsv-tk^{+} and $hENT1^{+}$ transgenes. Although the fission yeast strains were exposed to 0-, 6- and 24-hours of AZT/3TC drug treatment, only the mutation rate after 24-hours of drug exposure could be calculated (Figure 9). Several strains did not grow at all after 0- and 6-hours of exposure, resulting in values that did not fit the mutation rate model. After 24-hours of AZT/3TC exposure, the *rad3Δ* mutants had the highest mutation rate. In comparison with the mutation rates on complete media, the mutation rates on incomplete media were lower. This suggests that $his7^{+}$ or $leu1^{+}$ markers, and possibly the associated hsv-tk^{+} and $hENT1^{+}$ transgenes, were lost at a high frequency.

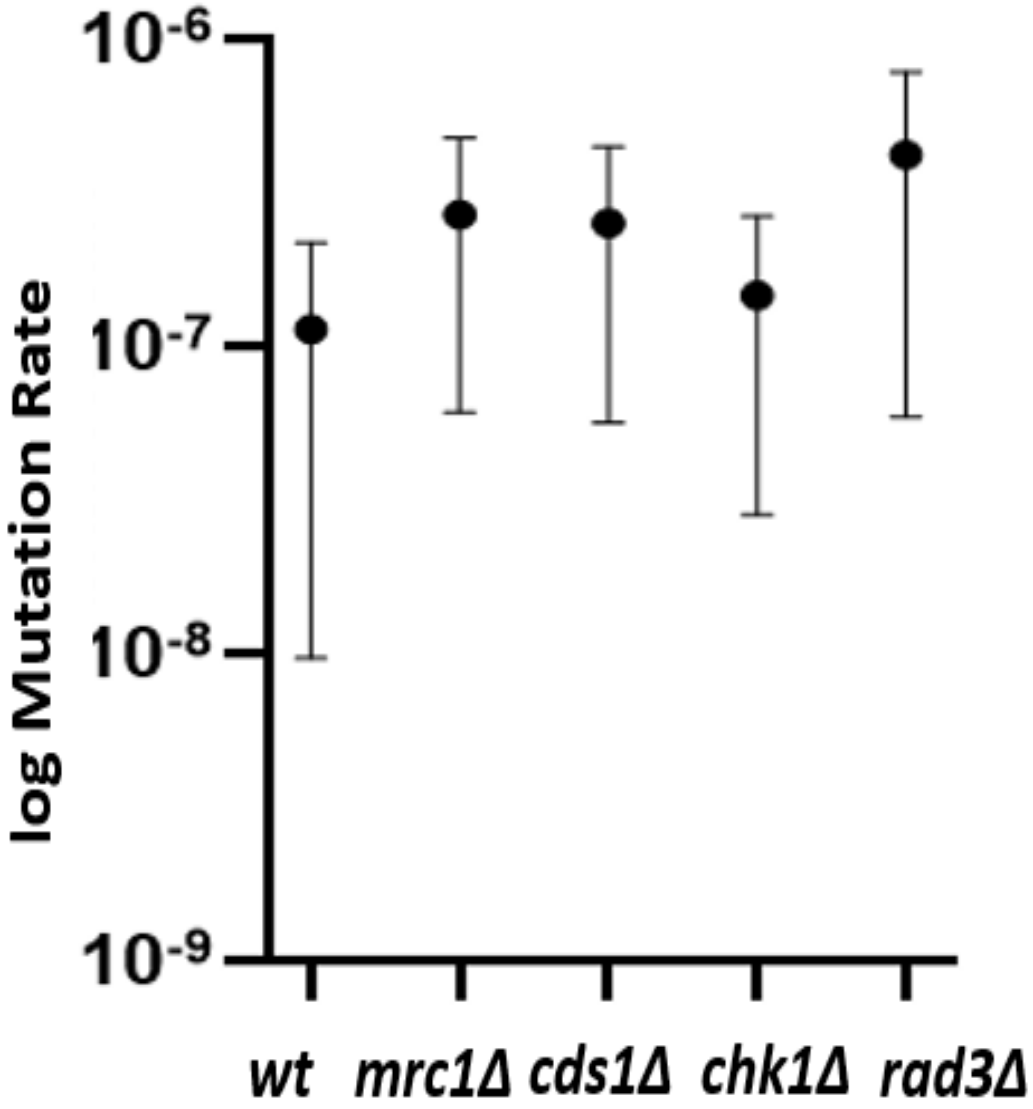

Figure 9. DNA mutation rate after AZT/3TC exposure with incomplete media. The mean DNA mutation rate after 24-hours of drug exposure was calculated over five experimental replicates in wildtype and cell cycle checkpoint fission yeast mutants. The mutation rate was highest for *rad3Δ* mutants. Error bars indicate 95% confidence intervals (n = 5).

4.1.3 Canavanine Mutation Frequency with complete media:

Using the data from Section 4.1.1, the mutation frequency was obtained using five experimental replicates and calculated for wildtype and checkpoint fission yeast mutants to assess colony growth on canavanine plates in comparison with the total number of cells plated. The mutation frequency was plotted on a logarithmic scale with upper and lower 95% confidence intervals (Figure 10). A difference in mutation frequency was not observed after 0- and 6-hours of AZT/3TC exposure in wildtype and checkpoint mutants. After 24-hours of drug exposure, the mutation frequency increased for all wildtype and checkpoint mutants.

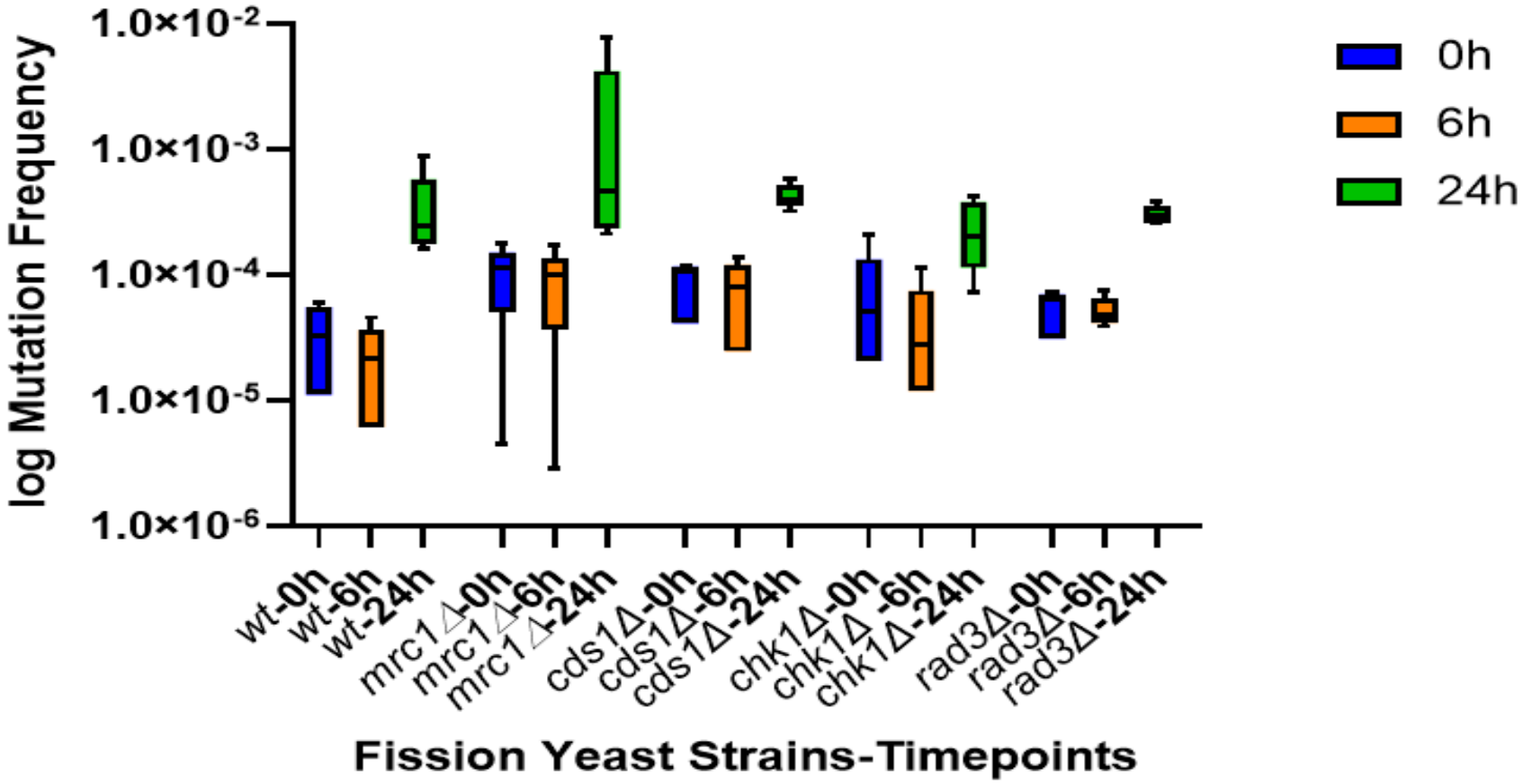

Figure 10. DNA mutation frequency with complete media. The average DNA mutation frequency was calculated over five experimental replicates by dividing the number of colonies on canavanine plates (with PMG-HULA) from the total number of fission yeast cells plated after AZT/3TC exposure. The mutation frequency did not differ between 0- and 6-hours of exposure. After 24-hours of exposure, the mutation frequency increased in wildtype and all checkpoint mutant cells. The box ranges from the 25th to 75th percentile and includes a line indicating the median. Error bars indicate 95% confidence intervals (n = 5).

4.1.4 Canavanine Mutation Frequency with incomplete media:

The mutation frequency was calculated as described in Section 4.1.2. The canavanine plates were made using incomplete media. Testing and comparing mutation frequencies in complete and incomplete media examines the importance of nutrient supplementation in media for a fission yeast model. Wildtype, *cds1Δ* and *chk1Δ* mutants had low mutation frequency levels at the 0-hour timepoint and then higher mutation frequency levels at the 6- and 24-hour timepoints, with no difference between the latter timepoints (Figure 11). The mutation frequency for *mrc1Δ* did not change with time. The mutation frequency for *rad3Δ* decreased after 6-hours of exposure and then increased again at the 24-hour timepoint, with no overall changes. The mutation frequencies for wildtype-0h, *cds1Δ*-0h, *chk1Δ*-0h and *rad3Δ*-6h was 0.

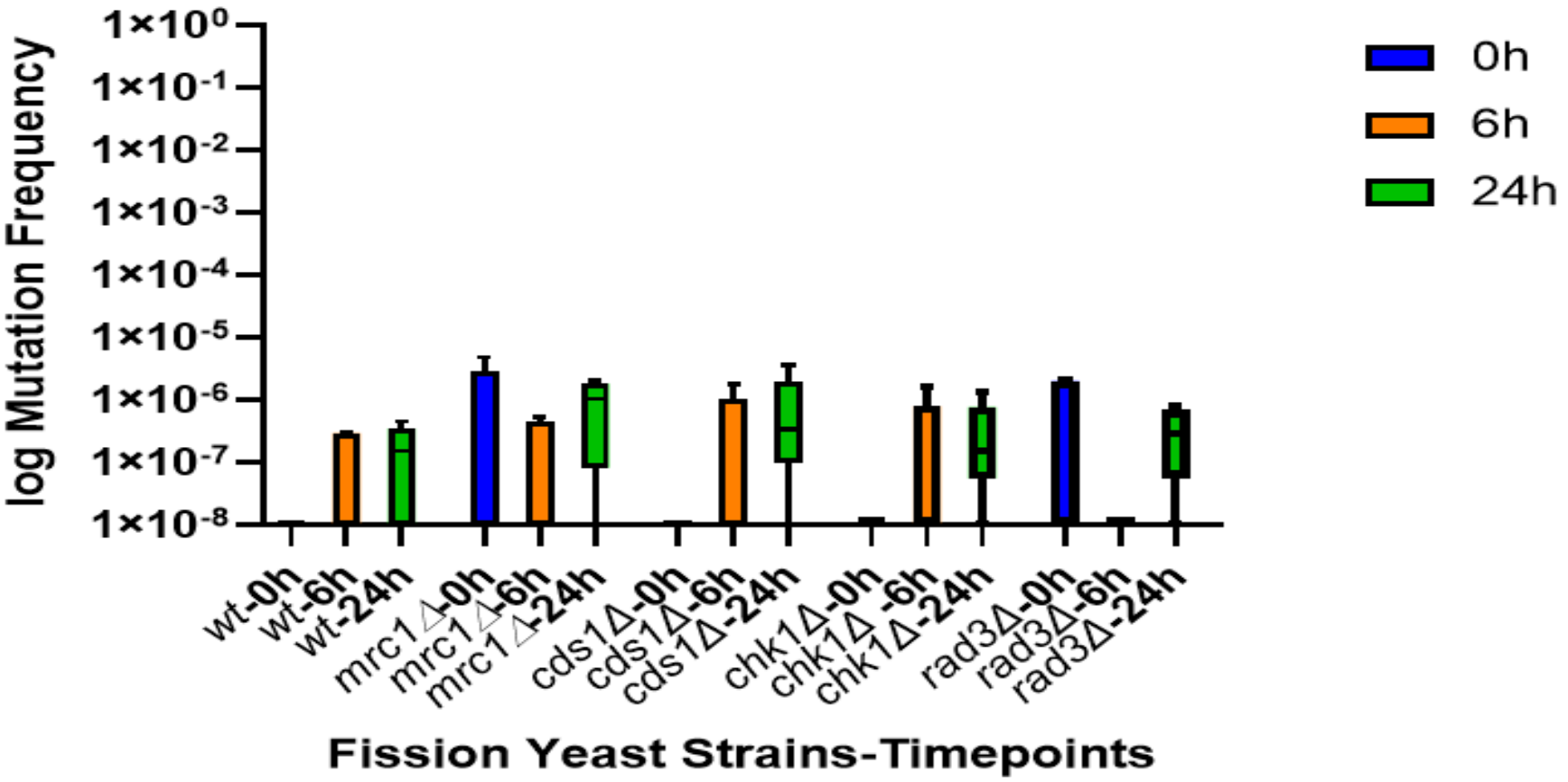

Figure 11. DNA mutation frequency with incomplete media. The average DNA mutation frequency was calculated using five experimental replicates based on the number of colonies on canavanine plates (with PMG-UA) relative to the total number of cells plated after Combivir (AZT+3TC) exposure. The mutation frequency did not differ between strains or timepoints. The box extends from the 25th percentile to the 75th percentile and includes the median as a line within the box. The whiskers range from the 5th percentile to the 95th percentile. Error bars indicate 95% confidence intervals (n = 5).

4.1.5 Assessment of Cellular Toxicity Using Trypan Blue:

The trypan blue dye stained dead wildtype and checkpoint mutant fission yeast cells a shade of blue. The average percentage of dead cells was assessed using ten replicates and was calculated by dividing the blue stained cells from the total number of cells observed. With the exception of *cds1Δ* after 6-hours and *rad3Δ* after 0-hours of AZT/3TC exposure, the average percentage of dead cells for all strains was below 30% (Figure 12). For wildtype and all checkpoint mutants, the percentage of dead cells after 0- and 6-hours of exposure was comparable, with a noticeable decrease observed after 24-hours of drug exposure. Differences were not observed between strains and timepoints.

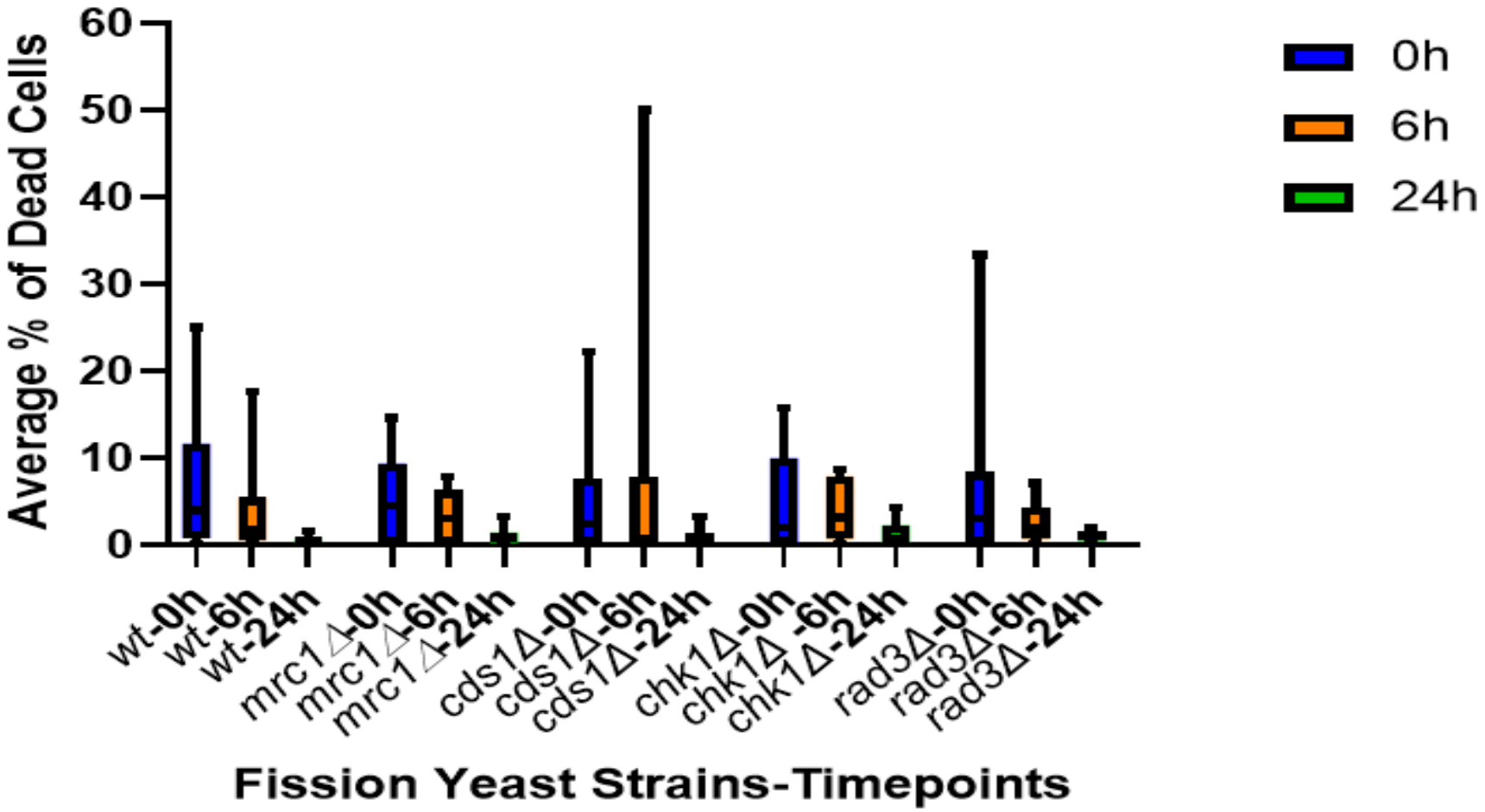

Figure 12. Average percentage of dead cells after AZT/3TC exposure. Fission yeast cells were exposed to Combivir (AZT+3TC) for 0-, 6-, and 24-hours. The average percentage of dead cells decreased after 24-hours of drug exposure but did not differ between strains or timepoints. The box ranges from the 25th to 75th percentile and includes a line indicating the median. Error bars indicate 95% confidence intervals (n = 10).

4.2 Effects of nucleoside analogs on gonads:

4.2.1 Assessment of H&E Stained Ovarian Follicles:

During fetal development, female germ cells enter meiosis and are known as oocytes. At birth, the oocytes remain arrested in meiosis I and are encircled by somatic cells making primordial follicles, which undergo folliculogenesis in sexually mature females.[78] The antral follicle count reflects reproductive potential.[88] To study the effects of cART exposure on germ cell and ovary development, we quantified the stages of folliculogenesis in mice exposed to ABC/3TC with ATV/r *in-utero* (Figure 13). The primary and secondary follicles were counted as one group. Antral follicles and corpus luteum were counted in separate groups. Primary and secondary follicles were lower in the cART group compared to the control, although this did not reach significance ($p = 0.123$). Antral follicles and corpus lutea were similar between groups ($p = 0.281$ and 0.227 respectively. Using chi-square test, a significant difference between the expected and observed frequencies of follicles was also not observed ($X^2 = 2.73$, $p = 0.255$). However, to improve statistical power, we need to increase our sample size and the number of quantified sections per ovary.

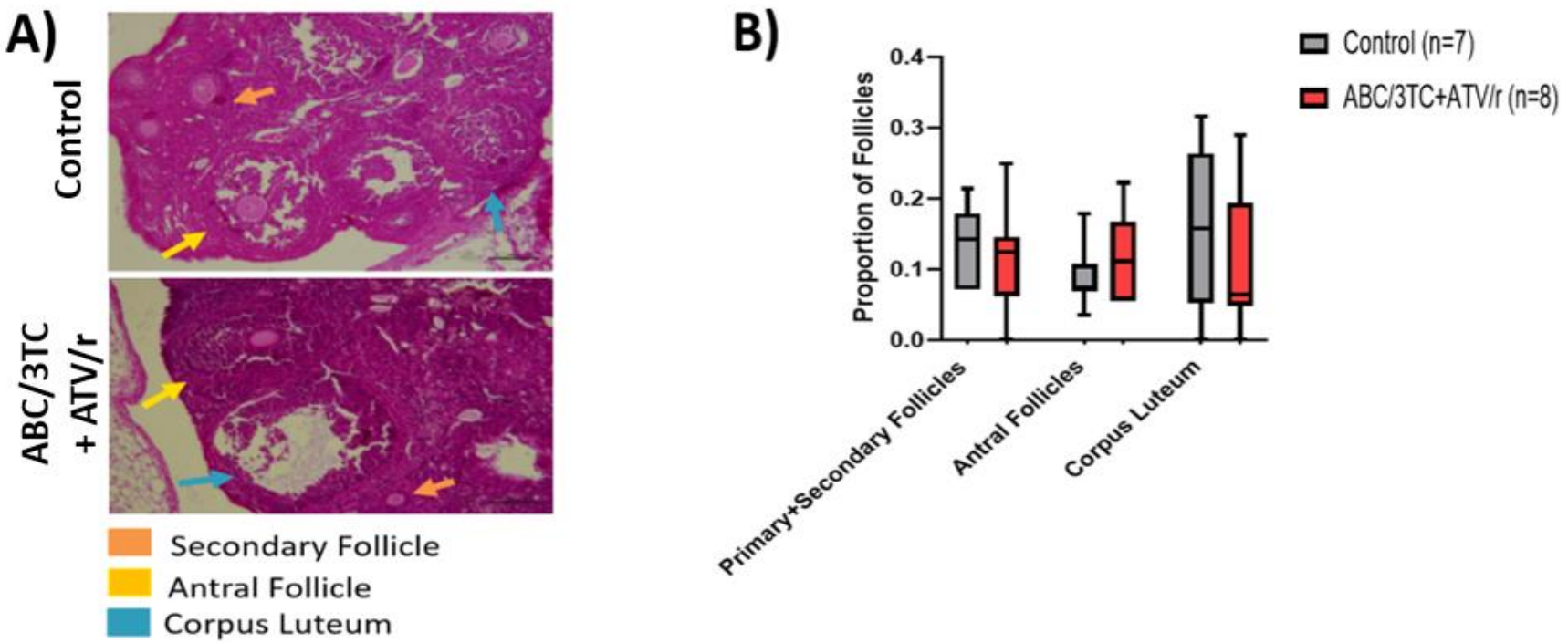

Figure 13. The effect of ABC/3TC with ATV/r on female germ cell development. A) Folliculogenesis stages were categorized as primary or secondary follicles, antral follicle, and corpus luteum. Scale Bars = 100 μm. **B)** Quantified stages of folliculogenesis are shown in a box and whiskers plots, with the line within the box indicating the median, and the box ranging from the 25th percentile to the 75th percentile. The whiskers extend from the 5th percentile to the 95th percentile. Differences in median values between treatment groups were evaluated using a two-tailed Mann-Whitney *U* test ($p < 0.05$). Differences in frequency distribution between treatment groups were evaluated using a chi-square test ($X^2 = 2.73$, $p = 0.255$). A significant difference after ABC/3TC with ATV/r exposure was not observed using either statistical test (n = 7 in control group; n = 8 in ABC/3TC with ATV/r group).

4.2.2 Assessment of H&E stained Testes:

4.2.2.1 Diameter of Seminiferous Tubules:

A qualitative assessment of the seminiferous tubules' histological structures revealed irregular lumen structure in testes exposed to ABC/3TC with ATV/r (Figure 14). Some seminiferous tubules in the treated samples were either missing a lumen or had a lumen that was localized to one end of the tubule. Seminiferous tubules from both control and treatment groups were lined with germinal epithelium. The average diameter of seminiferous tubules was not significantly different ($p > 0.05$) in the ABC/3TC with ATV/r treatment group.

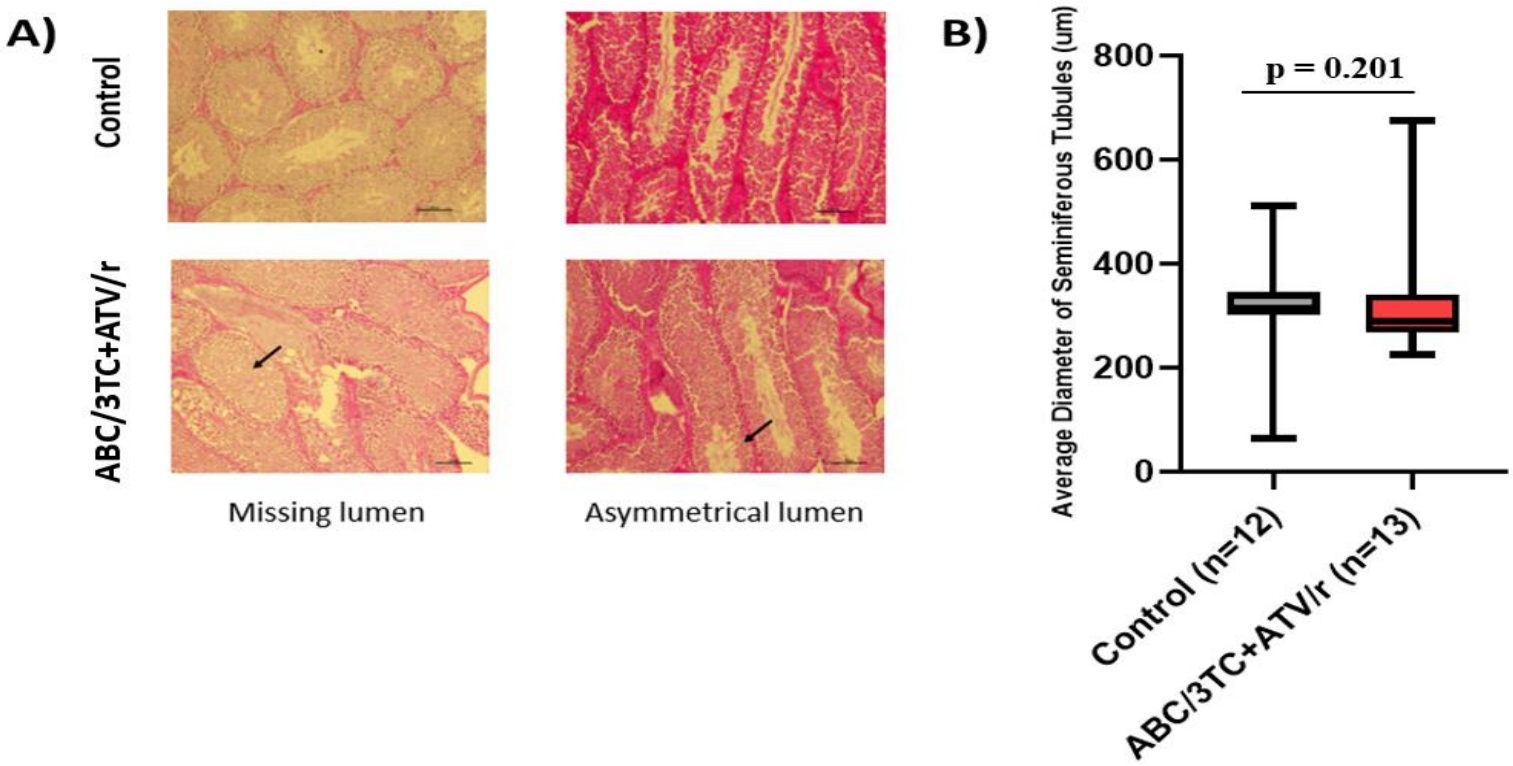

Figure 14. The effect of ABC/3TC with ATV/r on seminiferous tubule structure. A) H&E stained seminiferous tubules with missing and asymmetrical lumen in KIV+ATV/r treatment groups (x10). Bars = 100 μm. **B)** The average diameter of 20 seminiferous tubules in one section of a testis after exposure to ABC/3TC with ATV/r was plotting in a box and whiskers plot. The box extends from the 25th percentile to the 75th percentile and includes the median as a line within the box. The whiskers range from the 5th percentile to the 95th percentile. A two-tailed Mann-Whitney *U* significance test at the significance level 0.05 was performed to assess differences between groups (n = 12 in control group; n = 13 in ABC/3TC with ATV/r group).

4.2.2.2 Quantification of Sertoli and Leydig Cells:

Sertoli and Leydig cells were quantified by counting the respective cell type in ten random fields at a magnification of 40X (Figure 15). Sertoli cells were located inside the seminiferous tubules and were in direct contact with developing male germ cells. Leydig cells were observed in the connective tissue between seminiferous tubules. In the ABC/3TC with ATV/r treatment group, the number of Sertoli cells were significantly lower ($p < 0.05$) while the number of Leydig cells did not significantly differ from the control treatment group.

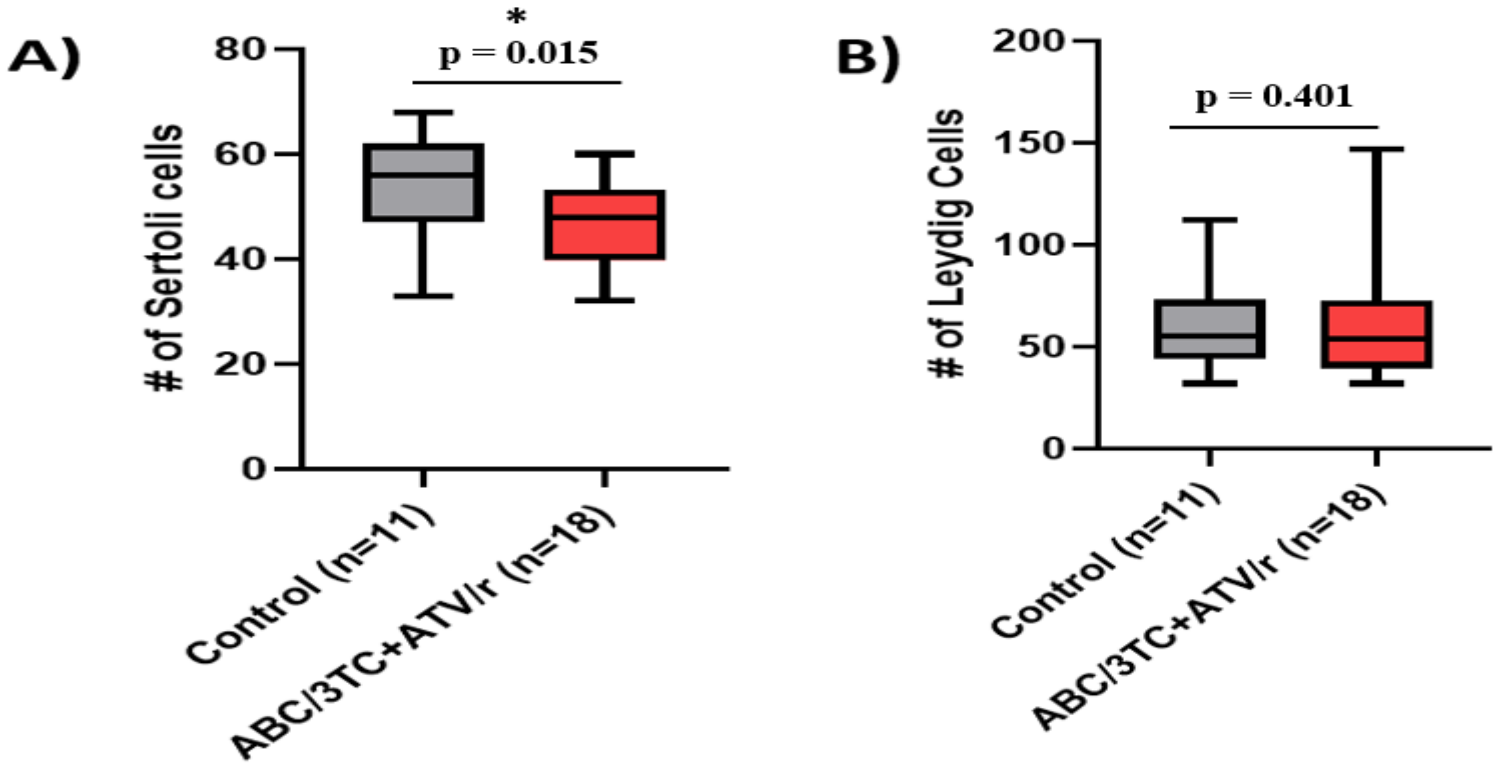

Figure 15. The effect of ABC/3TC with ATV/r on testis-specific cells. Number of Sertoli cells **(A)** and Leydig cells **(B)** in control (grey) and ABC/3TC with ATV/r treated (red) mice. A significant difference in the number of Sertoli cells between the control and the treatment group was observed while the number of Leydig cells were not statistically different after exposure to ABC/3TC with ATV/r. Data is presented using box and whiskers plots, with the line within the box indicating the median, and the box ranging from the 25th percentile to the 75th percentile. The whiskers extend from the 5th percentile to the 95th percentile (n = 11 in control group; n = 18 in ABC/3TC with ATV/r group). *Value significantly different than control group ($p < 0.05$, two-tailed Mann-Whitney *U* test).

4.2.2.3 Assessment of Epididymis:

The epididymis, a male reproductive organ connected to the testes, was qualitatively examined for histopathological markers associated with poor male fertility potential (Figure 16). The control group included 11 samples and the ABC/3TC with ATV/r treatment group included 6 samples. In both control and treatment conditions, the epididymal ducts were lined with epithelial cells. The epithelial cells did not appear degenerated and vacuoles in the epithelium were not detected in testes exposed to ABC/3TC with ATV/r treatment. Other markers like hyperplasia and sperm granulomas (masses of escaped spermatozoa lined with immune cells, white blood cells and granulation tissue[102]) were not observed.

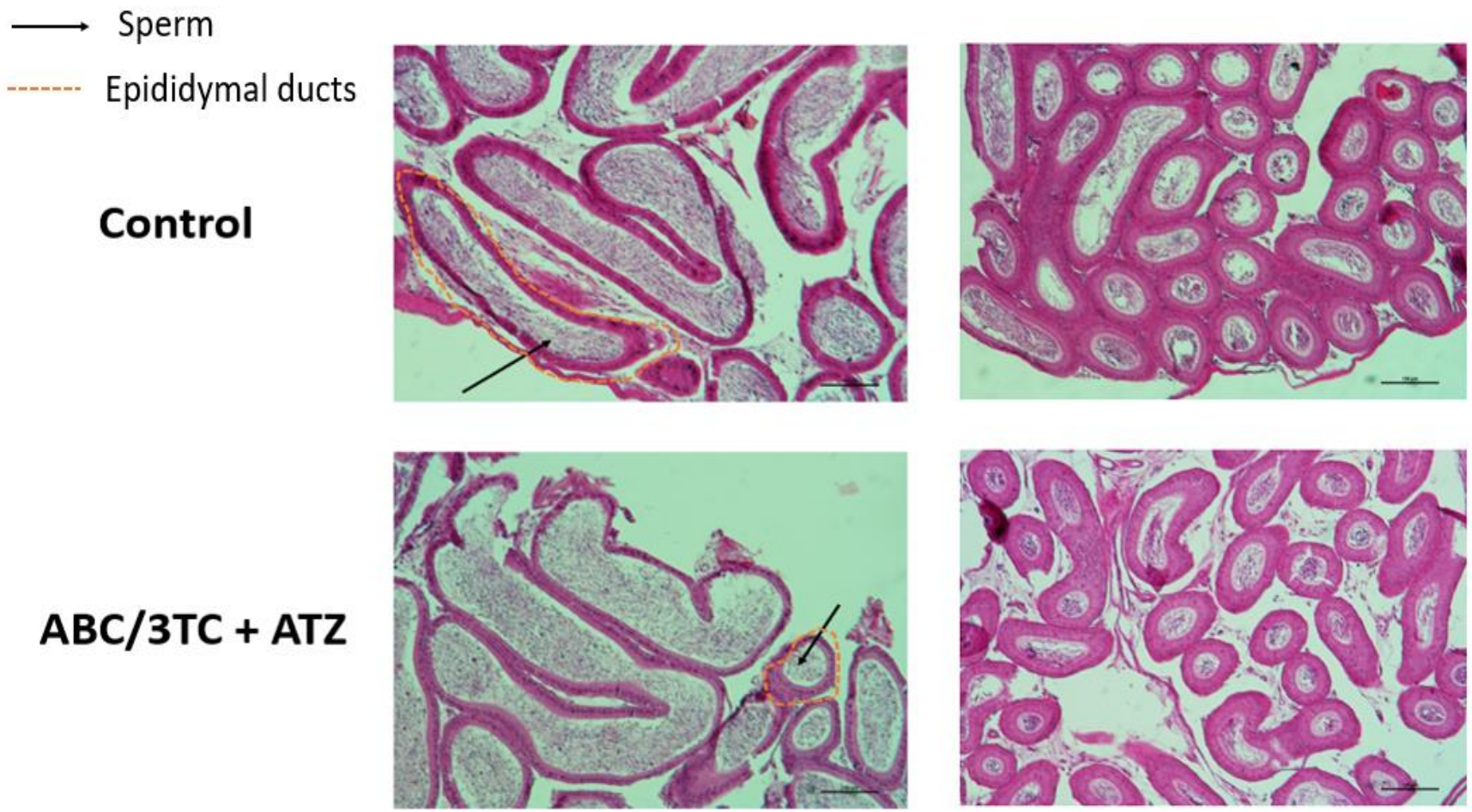

Figure 16. The effect of ABC/3TC with ATV/r on the epididymis. Sperm were present in epididymal tubules exposed to the ABC/3TC with ATV/r treatment (x10). Histopathological markers associated with reduced fertility potential were not observed. Scale Bars = 100 μm.

4.3 Summary of Findings:

For Aim I, the effects of nucleoside analogs on genomic stability were assessed by examining DNA mutations and cellular toxicity in a fission yeast model. We reported Rad3 sensitivity after 6 hours of AZT/3TC exposure which suggested the involvement of both the DNA damage and the DNA replication stress checkpoint pathways. We also reported an increase in mutation rate after 24 hours of AZT/3TC exposure, thus indicating genomic instability. The mutation rate in incomplete media could not be calculated after 0- and 6- hours of drug exposure due to lack of cell growth and the mutation rate for 24 hours was lower in incomplete media. Furthermore, we observed that cellular toxicity did not increase with long-term exposure to the dual NRTI AZT/3TC treatment.

For Aim II, we used a mouse pregnancy model to assess female and male germ cell and gonad development. We did not observe a significant difference in ovarian follicle numbers after exposure to ABC/3TC with ATV/r, which suggested normal female germ cell development. For male germ cell development, we reported no significant difference in seminiferous tubule diameter, Leydig cell number and epididymal health. However, we did observe low Sertoli cell numbers and altered seminiferous tubule morphology which indicated that male germ cell development may be affected. Our results for Aim II are limited due to sample size and we will improve our understanding by quantifying more sections of both male and female gonads.

5.0 DISCUSSION AND FUTURE DIRECTIONS

5.1 Effects of nucleoside analogs on genome stability:

5.1.1 Mutation Rate and Mutation Frequency after NRTI-exposure:

Fission yeast cell cycle regulation models the cell cycle control seen in mammalian cells.[106] Exposure to genotoxic stress like drug exposure can activate DNA damage- or DNA replication stress-specific cell cycle checkpoint proteins, which prevent cell cycle progression.[110] Given the similarity of its molecular and genetic mechanisms, fission yeast is a well-established model organism for testing drugs like nucleoside analogues.[105]

After exposure to AZT/3TC, canavanine mutation rate assays with complete and incomplete media were used to assess genomic stability after 0-. 6- and 24-hours of exposure (Figure 8 & 9). On the standard complete media, the mutation rate after 6-hours of exposure was only higher for *rad3Δ* mutants. The mutation rate increased considerably after 24-hours of drug exposure for all strains. The higher mutation rate for *rad3Δ* mutants after a shorter duration of drug exposure is expected considering that the kinase Rad3 mediates both the DNA replication stress and DNA damage pathways. DNA damage has previously been reported after AZT/3TC exposure.[33] High mutation rates occur due to activation of the DNA replication stress checkpoint pathway in fission yeast.[118] Increases in mutations have also been reported after AZT/3TC treatment *in vitro* and *in vivo*.[34] Thus the sensitivity of *rad3Δ* mutants and the activation of both DNA replication stress and the DNA damage pathways in fission yeast are supported by the reported genotoxic effects of the AZT/3TC treatment.

For the canavanine mutation rate assay on incomplete media, the mutation rate could not be calculated after 0- and 6- hours of drug exposure due to the lack of colonies detected on incomplete media in the concentrations and conditions used. The mutation rate after 24-hours of

drug exposure was the highest for *rad3Δ* mutants but was still lower than the mutation rates calculated from complete media. Our results indicate that fission yeast cells plated on media without histidine and leucine had mutations impacting histidine and leucine markers causing cell death. Considering that histidine and leucine prototrophy may be lost, the mutation rate appears to be lower than the complete media mutation rate, as cells are unable to survive on the incomplete media and hence cannot become sensitive or resistant to canavanine. Thus, our results emphasize the importance of calculating mutation rate from complete media as cells on incomplete media do not survive to experience the effects of canavanine.

Mutation rate (m/N_t) is calculated by dividing the number of mutational events (m) by the total number of viable cells (N_t). It predicts the number of mutations in a cell per cell division or generation. [119,120] Mutation frequency (r/N_t) is calculated by dividing the number of mutants (r) by the total number of viable cells (N_t).[119] The mutation rate model for fluctuation assays was originally proposed by Luria and Delbrück and has since been expanded by Lea and Coulson.[120] Its validity relies on several assumptions including the accurate observation and identification of all mutants, and an exponential cell growth rate, which is consistent between nonmutants and mutants. Reverse mutations and cell death are considered negligible. Furthermore, the likelihood of mutational events is considered constant in each generation and independent of earlier mutations.[120]

Since mutation rate is calculated using a mathematical model that considers fluctuation analysis, and as a result, predicts DNA changes with time, it provides a more accurate assessment of genome stability than mutation frequency. However, although mutation frequency is less accurate and cannot account for spontaneous mutations, it is still considered a useful measurement for assessing mutations induced by drugs.[119] The mutation frequency was calculated for mutants

growing on canavanine plates with complete and incomplete media. For the assay with complete media, the mutation frequency significantly increased after 24-hours of *Combivir* exposure for wildtype and checkpoint mutants (Figure 10). This indicates that the dual NRTI treatment activates both the DNA damage and the DNA replication stress checkpoint pathways.

There was a significant difference between the mutation frequencies calculated from mutants growing on complete and incomplete media. For the assay with incomplete media, several strains had a mutation frequency of 0, as mutants were unable to grow on canavanine plates with PMG-UA (Figure 11). Furthermore, there were no significant differences observed between strains and timepoints. These results highlight the importance of nutrient supplementation when linked to prototrophic markers. Loss of either the $his7^{+}$ or $leu1^{+}$ markers during drug exposure would render cells unable to grow on the incomplete medium. Since these are functionally linked to the transgenes for analogue uptake and processing, this implies that AZT and 3TC impose selective pressure during exposure. Overall, our results support the current standard approach to a canavanine mutation rate assay which uses a complete permissive media with all supplements (HULA) to ensure that environmental stress or drug-induced genetic instability does not affect nutrient availability.

Unpublished work from the Sabatinos lab (Su, C. in preparation, Ryerson University 2018) has assessed genomic stability on incomplete media after short-term (0- and 6-hours) exposure to AZT and 3TC alone in wildtype fission yeast. An increase in *can1* mutations was observed after 6-hours of AZT exposure while a significant difference in the mutation rate was not observed after 6-hours of 3TC exposure. Although the mutation rate on incomplete media in wildtype fission yeast after 0- and 6-hours of AZT/3TC exposure could not be calculated, the mutation rate after

24-hours of drug exposure was the highest for *rad3Δ* mutants, indicating both DNA damage and DNA replication stress genotoxic effects.

The mutagenic effects of AZT monotherapy in human cells are well-established.[32,85] To mitigate these effects, the use of a second NRTI, such as 2',3'-dideoxyinosine (ddI) has been investigated. However, a synergistic effect on genomic instability has been reported after AZT-ddI therapy.[32] The effect of AZT monotherapy, 3TC monotherapy and dual-NRTI (AZT/3TC) treatment on genomic stability has been studied in the context of the *in vivo* mutation rate HIV-1.[122,123] In two separate studies, HeLa target cells were respectively pre-exposed to AZT monotherapy, 3TC monotherapy and combined AZT+3TC treatment for 2 hours, infected with HIV-1, and then treated with the previous respective drug treatment for 24-hours. The HIV-1 mutation rate increased by a factor of 7 after AZT exposure and by a factor of 3 after 3TC exposure.[122] These results follow the same trend demonstrated by the Sabatinos lab, where AZT monotherapy was established as more mutagenic than 3TC monotherapy. Interestingly, the study focusing on combined AZT+3TC treatment reported the greatest increase in mutation rate after exposure to the dual NRTI treatment, where the HIV-1 mutation rate increased by a factor of 9.[123] Given our finding of an increased mutation rate on complete media after long-term (24h) of AZT/3TC exposure and unpublished work from the Sabatinos lab indicating AZT being more mutagenic than 3TC after short-term (6h), it can be inferred that AZT-based NRTI combinations promote genomic instability during both short and long-term exposure.

Considering that our results support the use of complete media for canavanine mutation rate assays and that the canavanine mutation rate assays with AZT and 3TC alone (Su, C. In Preparation, Ryerson University 2018) were performed on incomplete media, we will repeat the assays on complete media to compare the short-term effects of single NRTI regimens with dual-

NRTI combinations. For future experiments, we will also sequence the *can1* mutants to check for loss of *can1* function. Furthermore, we will use hydroxyurea, an anti-cancer drug that also activates fission yeast's DNA replication stress checkpoint pathway and causes reversible cell cycle arrest in early S-phase as a positive control.[118,124] By targeting the enzyme ribonucleotide reductase, HU reduces the available pool of deoxynucleotide triphosphates (dNTPs), which in turn contributes to replication fork instability, damages DNA and ultimately leads to replication fork collapse.[118]

5.1.2 Cellular Toxicity after NRTI-exposure:

The colorimetric trypan blue dye stains dead cells by entering dead cells through their non-functional membranes. Viable cells remain unstained.[125] The average percentage of dead cells after AZT/3TC exposure did not significantly differ among strains or timepoint (Figure 12). This is inconsistent with reported literature, as low cell survival after *in vitro* exposure to AZT/3TC has been reported.[104] A major concern surrounding AZT/3TC's toxicity is its effect on mitochondrial damage,[25] with one study reporting high mitochondrial DNA damage after AZT/3TC treatment in mice.[126] Although our data suggests that AZT/3TC treatment does not increase cellular toxicity over time, given the existing literature surrounding mitochondrial damage, this may require future investigation in other models. Further, the effect of AZT/3TC on cell viability recognized by Trypan Blue might only be visible once membrane disruption is established, and might therefore be detected at a later time point.

5.2 Effects of cART on germ cell development:

5.2.1 Quantification of H&E Stained Ovarian Follicles:

With primordial germ cell development starting before birth and children being exposed to cART since conception, we are concerned about the effects of cART on meiosis.[48,78] To study

these effects, we completed a histological assessment of male and female gonads from mice exposed to ABC/3TC with ATV/r treatment *in-utero*. In females, we focused on quantifying the stages of folliculogenesis. At birth, the ovaries have primordial follicles which contain female germ cells, also known as primary oocytes, arrested in Meiosis I.[78,83] In sexually mature females, reproductive hormones trigger the menstrual cycle, where select primordial follicles undergo follicular development.[78,82] During this process, the germ cells within the follicles also complete meiosis I and arrest in meiosis II.[81] The stages of folliculogenesis include antral follicles, which are considered a biomarker for ovarian aging, with the number of antral follicles being proportional to the rate of fertility.[88] In our preliminary analysis, we used a two-tailed Mann-Whitney *U* test and a chi-square test to determine that the number of primary and secondary follicles, antral follicles and corpus luteum were not affected after *in utero* exposure to ABC/3TC with ATV/r treatment (Figure 13). Although counting the number of follicle numbers in mice is an established experimental system for studying reproductive health, counting protocols and as a result, correction factors and the number of reported follicles in each stage of folliculogenesis varies with each study.[127,128] One study that assessed the variability of reported follicle numbers and studied ovaries of wild-type female C57BL/6/128SvEv mice at 100 days of age reported 265 $\pm$ 32 primary follicles, 79 $\pm$ 5.6 secondary follicles, 40 $\pm$ 4.8 early antral follicles and 15.6 $\pm$ 2.3 antral follicles per ovary.[128] After quantifying more sections within our ovary samples, we will compare our follicle numbers from the control group to determine whether they reflect the follicle numbers reported in literature.

The current literature focusing on female fertility primarily examines the effects of HIV viral infection, and not NRTIs, on fertility, with reports of reduced female fertility potential from untreated advanced HIV infections.[129] Although clinical fertility outcomes of children exposed to

NRTIs is lacking, sex steroid hormone levels relevant to fertility have been examined in the context of pregnancy. Progesterone is required for maintaining pregnancy and fetal growth, as well as regulating ovarian processes like folliculogenesis and ovulation.[55,130] The Serghides lab has used *in vitro* and *in vivo* models to show that single and dual NRTI regimens do not contribute to lower progesterone levels and adverse pregnancy outcomes. However, when NRTIs are combined with the protease inhibitor Kaletra (ritonavir-boosted lopinavir), clinical outcomes include low progesterone levels, low fetal weight and low placental weight.[55] Our results examining the effects of ABC/3TC with ATV/r are limited by sample size. Thus, determining the effect of NRTIs with ATV/r on meiotic development remains an area of active investigation with future studies possibly expanding to also look at the effects of progesterone levels and pregnancy outcomes. In these future investigations, we will increase our sample size and the number of sections counted per sample to improve our overall examination of reproductive and fertility health outcomes after cART-exposure.

5.2.2 Assessment of H&E Stained Testes:

The impact of antiretroviral therapy on male fertility has been studied, although a knowledge gap still exists in the context of meiotic development and testicular structure. In the testes, seminiferous tubules with smaller diameters are an indication of lower germ cell numbers and/or loss of seminiferous tubule fluid.[93] Located between seminiferous tubules, Leydig cells make the sex steroid hormone testosterone.[97] Sertoli cells are activated by FSH and have many functions, including being necessary for testis formation and secreting androgen binding protein, which in turn directs testosterone to the seminiferous tubule lumen. As a result, testosterone can regulate meiotic completion, maintain the blood-testis barrier for nutrient transportation, discharge

mature sperm from Sertoli cells to prevent sperm phagocytosis and control the Sertoli cell-specific secretion of the seminiferous tubule fluid forming the lumen.[97]

A quantitative analysis of testes exposed to ABC/3TC with ATV/r *in utero* demonstrated no significant difference in seminiferous tubule diameter and the number of Leydig cells while the number of Sertoli cells were significantly lower in comparison with the control group (Figure 14 & 15). These preliminary findings suggest that testosterone production may not be impacted but testosterone levels within the seminiferous tubules may be affected given the lower number of Sertoli cells. Moreover, considering that some seminiferous tubules had missing or irregularly localized lumens in the treated testes group, germ cells may have limited access to testosterone, which in turn could impair the previously discussed functions of testosterone.

Other studies assessing the importance of Sertoli cell numbers have found that complete ablation or even partial reduction in Sertoli cell population adversely impacts spermatogenesis, as well as germ cell and Leydig cell numbers in mice.[131,132] Our pilot study has a low statistical power as only one section of each testis sample was counted. Hence, improving statistical power by increasing the number of quantified sections will improve our understanding of the effects of cART exposure on testis-specific cells and overall germ cell development.

Low testosterone levels, also known as hypogonadism, have been reported in men with HIV but a significant difference has not yet been observed between PI, NRTI and NNRTI treatments.[133,134] Considering that the number of Leydig cells are not affected by ABC/3TC with ATV/r exposure, our preliminary results suggest that baseline testosterone production in mice exposed *in utero* may not be affected. To gain more insight about the molecular mechanisms of male fertility outcomes, future experiments could examine testicular homogenates using an enzyme immunoassay to determine testosterone levels after PI-cART exposure.[135] Our preliminary

results indicate that testosterone levels in the testes of male mice exposed to ABC/3TC with ATV/r *in utero* would not significantly differ from males in the control group.

A qualitative assessment of the epididymis for histopathological markers of reduced fertility demonstrated no significant difference between the control and the ABC/3TC with ATV/r treatment groups (Figure 16). The epididymis was examined for epithelial cell degeneration, intra-epithelial vacuole formation, hyperplasia and sperm granulomas. These preliminary findings suggest a minimal impact on sperm maturation and storage, the main functions of the epididymis.[98] However, to conclusively state the effects of the ABC/3TC with ATV/r treatment on the epididymis, we will increase our sample size. Moreover, to further investigate these effects, a quantitative assessment can also be conducted by measuring the diameter of epididymal tubules and the height of the epithelial cells. A reduction in these quantitative markers is associated with androgen deprivation and has been observed after exposure to toxicants that inhibit Leydig cells' ability to synthesize testosterone.[136] Thus a quantitative assessment of the epididymis from a larger sample size will provide greater insight about the effects nucleoside analogs on male gonad development and fertility potential.

6.0 CONCLUSIONS

With cART being necessary for preventing vertical transmission of HIV and current treatment guideline exposing children to cART from conception[48], we assessed the effects of *in-utero* cART exposure on the reproductive health of offspring. Using our fission yeast model, we examined genomic stability in Aim I. We used a canavanine mutation rate assay and reported the use of complete media for calculating accurate canavanine mutation rates. We also observed Rad3 sensitivity, which indicated the involvement of both the DNA damage and DNA replication stress checkpoint pathways after short-term AZT/3TC exposure. We reported higher mutation rates indicating a greater impact on genomic stability after long-term AZT/3TC exposure. For cellular toxicity, we reported that exposure to AZT/3TC does not increase in toxicity over time. For Aim I, we hypothesized an increase in DNA mutations and cellular toxicity after NRTI-exposure. Our results partly support our hypothesis as both mutation rate and frequency increased with long-term exposure to the dual-NRTI treatment, while cellular toxicity was not increased. Thus, we conclude that the AZT/3TC nucleoside analog combination promotes mutagenicity but does not increase in toxicity over time.

For Aim II, using our mouse pregnancy model, we assessed how *in-utero* cART exposure affects male and female gonad development. We hypothesized low ovarian follicle numbers after *in-utero* exposure to anti-HIV drugs. Our preliminary assessment of female gonads does not support our hypothesis as cART exposure did not affect the number of ovarian follicles, thus indicating normal female germ cell development and female reproductive health. We also hypothesized disrupted testis structure, thus indicating poor male reproductive health after *in-utero* cART exposure. Our preliminary work with male gonads from mice exposed to cART *in-utero* partly supports our hypothesis as we observed no effect on the diameter of seminiferous tubules,

on epididymal health or on the number of Leydig cells but lower Sertoli cell numbers and missing or irregularly localized lumens in seminiferous tubules were reported. We speculate that this may suggest normal testosterone production but altered testosterone levels within the seminiferous tubules, which in turn would adversely impact male germ cell development and male fertility.

Given our assessment of genomic stability as well as the data reported in existing genotoxic studies, we conclude that AZT-based NRTI combinations should not be included in cART regimens taken during pregnancy. Our examination of germ cell development concludes that the ABC/3TC NRTI combination may have sex-specific effects on the reproductive health of offspring, with male offspring reproductive potential being at a greater risk than female. We recognize that our assessment of male and female germ cell development effects is limited due to sample size and we will improve our understanding by quantifying more sections of both male and female gonads. We also aim to expand our study by testing more NRTI combinations to ultimately find the safest NRTI combinations for use during pregnancy.

Understanding the effects of NRTI-exposure on genomic stability and of *in-utero* cART exposure on male and female germ cell development will lead to a better understanding of how older and existing anti-HIV drugs impact fertility. By assessing the impact of historical backbone NRTI combinations like AZT/3TC as well as existing cART regimens like ABC/3TC with ATV/r, this research lays the groundwork for identifying the safest NRTI combinations for pregnant women living with HIV and for determining whether children previously exposed *in-utero* are at risk for fertility issues. Hence, it has implications for HIV treatment guidelines during pregnancy, fertility treatments for people living with HIV and family planning for children exposed to anti-HIV drugs *in-utero.*

7.0 APPENDIX

In this appendix, we discuss completed methods as well as a future nested-PCR design that will be used to analyze DNA methylation in tail and sperm samples from mice exposed to anti-HIV drugs *in-utero*. We hypothesize that i*n-utero* exposure to anti-HIV drugs will be associated with aberrant DNA methylation patterns, thus indicating reduced reproductive potential and poor fertility.

7.1 DNA Methylation Analysis Using Bisulfite Sequencing:

To isolate genomic DNA from mouse tail and sperm samples, SNET lysis buffer was prepared by mixing 400 mM of sodium chloride (NaCl), 1% (w/v) of sodium dodecyl sulfate, 20 mM of Tris hydrochloric acid (Tris-HCl) at pH 8.0, and 5 mM of ethylenediamine tetraacetic acid (EDTA) at pH 8.0 (BioShop, Burlington, Canada). The buffer was filter sterilized using a 0.22 μm nitrocellulose filter. The lysis buffer with 400 μg/mL of proteinase K was added to each tissue sample and then incubated overnight at 55°C. A 1:1 volumetric ratio of phenol:chloroform:isoamyl alcohol and the buffered sample was centrifuged at 11,000 revolutions per minute (RPM) for 5 minutes. Equal volumes of the sample's aqueous phase and chloroform (BioShop, Burlington, Canada) were added to a microcentrifuge tube containing approximately 100 μL of vacuum grease (Dow Corning, Michigan, United States) and centrifuged at 11,000 RPM for 5 minutes. In a fresh microcentrifuge tube, equal volumes of the sample's upper aqueous layer and isopropanol were combined to precipitate the DNA. The mixture was stored in -20°C for 5 minutes and then immediately centrifuged at 13,000 RPM for 10 minutes. After discarding the supernatant, the precipitated DNA was washed with 1 mL of 70% ethanol. The samples were centrifuged at 13,000 RPM for 5 minutes. Once the ethanol was removed, the DNA pellets were air-dried at room

temperature for 5 minutes, and then re-suspended in 100 μL of Tris-EDTA (TE) buffer (pH 8.0). The samples were stored at 4°C. For nucleic acid quantification a NanoDrop Spectrophotometer was used, with 2 μL of TE buffer as a blank (Table S1).

CpG methyltransferase (New England BioLabs, Whitby, Canada) was prepared by combining 1X NEBuffer 2 with 160 uM of S-adenosylmethionine (50 mM of NaCl, 10 mM of Tris-HCl, 10 mM of magnesium chloride ($MgCl_2$) and 1 mM of dithiothreitol) and added to a control mouse trail sample. After a 60-minute incubation at 37°C, the enzyme was inactivated via heat exposure at 65°C for 20 minutes.

Using the EZ DNA Methylation Gold Kit (Zymo Research, California, United States), the CT Conversion Reagent and the M-Wash Buffer were prepared as outlined by the kit's protocol. The DNA samples were mixed with 130 μL of the CT Conversion Reagent. In a thermal cycler, the samples were exposed to 98°C for 10 minutes, 64°C for 2.5 hours and then stored overnight at 4°C. The DNA samples and 600 μL of the M-Binding Buffer were then added to a collection tube's Zymo-Spin 1C column, mixed and centrifuged at 13,000 RPM for 30 seconds. After disposing the flow-through, 100 μL of the M-Wash Buffer was added and centrifuged at 13,000 RPM for 30 seconds. Following the addition of 200 μL of M-Desulphonation Buffer and a 15-minute incubation at room temperature, the samples were centrifuged at 13,000 RPM for 30 seconds. The samples were then washed with 200 μL of M-Wash Buffer and centrifuged at 13,000 RPM for 30 seconds. In a microcentrifuge tube, 10 μL of the M-Elution Buffer was loaded in the column and then centrifuged at 13,000 RPM for 30 seconds. All samples were stored at -20°C for polymerase chain reaction (PCR).

Table A1. The quantification DNA in mouse tail and sperm samples.

Sample	Nucleic Acid Concentration (ng/µL)	$A_{260/280}$
BD3A	98.6	1.90
BE3A	184.8	1.87
BD4A	141.8	1.86
BD4B	111.1	1.90
BD3B	87.4	1.86
BE3B	193.4	1.85
BR1	46.6	2.05
BR2	52.8	2.05
BR3	107.5	2.04
BR4	75.9	2.03
BT0	56.8	2.03
BO2	73.4	2.04
BE1	67.5	2.10
BV0	89.5	2.06
BT4	165.4	2.03
BV4	36.5	2.09
BO0	81.8	2.05
BO4	109.5	1.98
BO3	88.7	1.98
BE3	78.9	1.89
BE2	239.0	1.91

BN1	41.9	1.90
BN3	46.0	1.93
BE4	144.7	1.92
BN2	6.60	2.33
BH4	32.8	2.13
BH3	72.3	2.19
BH1	62.5	2.25
A	62.5	2.67
B	112.9	2.01
BV3	98.7	2.11
BH2	96.5	2.00

The concentration of DNA from mouse tail and sperm samples in control and ABC/3TC with ATV/r treatment groups was quantified. The absorbance ratio of 260 nm and 280 nm was used to determine sample purity, with $A_{260/280}$ ratios of approximately 1.8 considered largely free of protein contamination.[137]

7.1.1 PCR Primer Design:

A nested PCR assay will be performed to amplify the imprint control region of H19-Igf2 (GenBank Accession no. U19619.1).[138] Using Primer-BLAST, specific primer pairs were selected (Table S2). For the first round of PCR, the reverse primer from primer pair 3 and the forward primer from primer pair 10 will be used to obtain the first amplicon (Figure S1). For the second round of PCR, the forward and reverse primers of primer pair 5 will be used.

Table A2. Nested-PCR Primers.

Primer Pair	**Primer Sequences (5'→3')**
Primer 3	Forward: ACCAGTGCATGTGGTTCGAT
	Reverse: GACGATCTCGGGCTGTGTAG
Primer 5	Forward: GGGGGTCACAAATGCCACTA
	Reverse: CCGGGACAGTGCAAAAACAG
Primer 10	Forward: AGCCATTGCCTACAGTTCCC
	Reverse: GCCTCATGAAGCCCATGACT

The reverse primer from the primer pair 3 and the forward primer from the primer pair 10 will be used as the outer pair of primers. Both forward and reverse primers of primer pair 5 will be used as the inner primers.

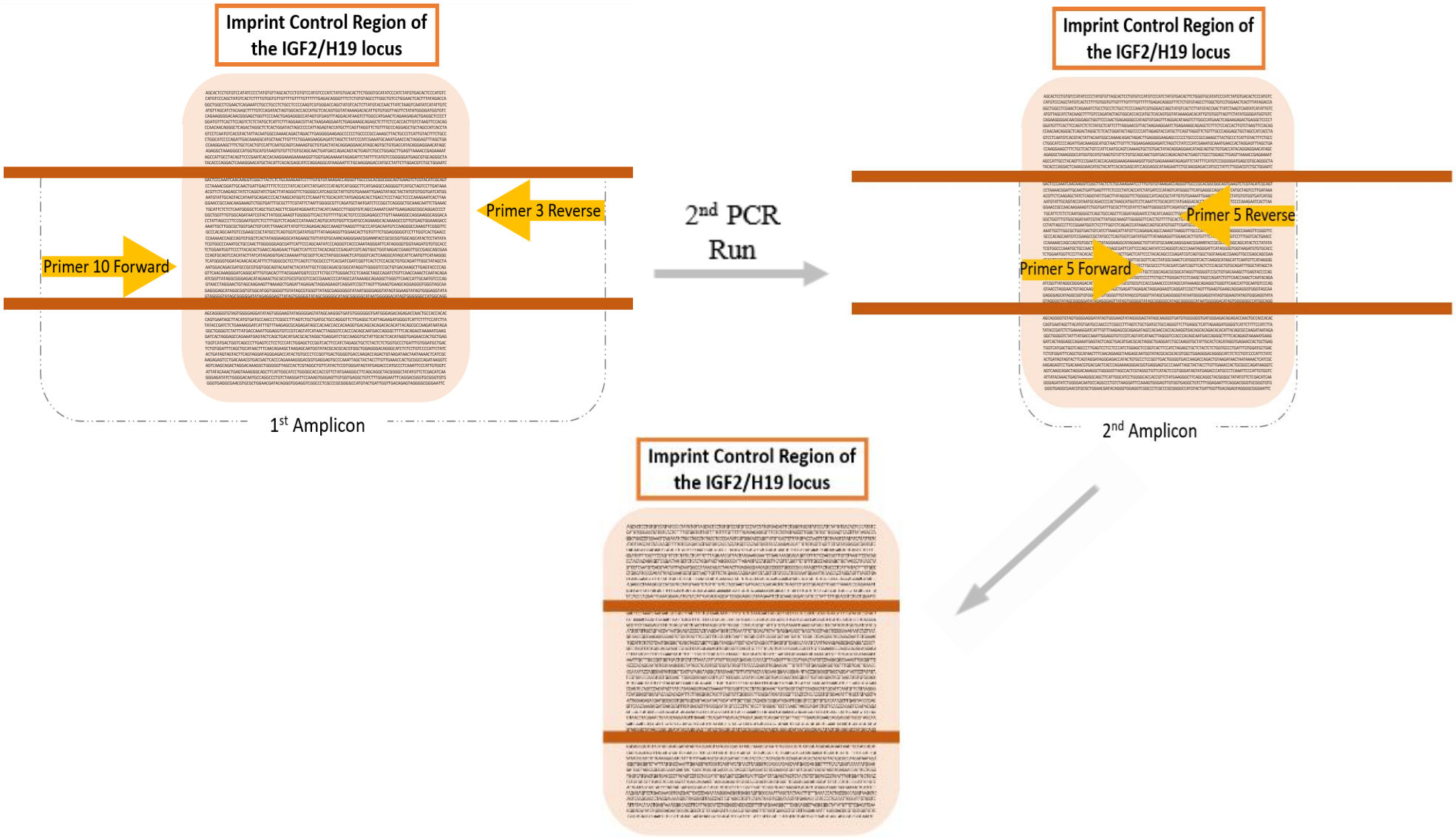

Figure A1. Schematic diagram of Nested PCR. This assay will use a set of outer and inner primers to improve the specificity of DNA amplification in the imprint control region of the IGF2/H19 locus.

8.0 REFERENCES

1. Levy, J. A. Pathogenesis of human immunodeficiency virus infection. *Microbiol. Rev.* **57**, 183–289 (1993).
2. Tang, H., Kuhen, K. L. & Wong-Staal, F. Lentivirus Replication and Regulation. *Annu. Rev. Genet.* **33**, 133–170 (1999).
3. Global HIV & AIDS statistics — 2019 fact sheet. https://www.unaids.org/en/resources/fact-sheet.
4. Hladik, F. & McElrath, M. J. Setting the stage – HIV host invasion. *Nat. Rev. Immunol.* **8**, 447–457 (2008).
5. Nakamura, K. J. *et al.* Breast milk and in utero transmission of HIV-1 select for envelope variants with unique molecular signatures. *Retrovirology* **14**, (2017).
6. Marinda, E. *et al.* Child mortality according to maternal and infant HIV status in Zimbabwe. *Pediatr. Infect. Dis. J.* **26**, 519–526 (2007).
7. Connor, E. M. *et al.* Reduction of Maternal-Infant Transmission of Human Immunodeficiency Virus Type 1 with Zidovudine Treatment. *N. Engl. J. Med.* **331**, 1173-1180 (1994).
8. Life expectancy of individuals on combination antiretroviral therapy in high-income countries: a collaborative analysis of 14 cohort studies. *Lancet* **372**, 293–299 (2008).
9. Papp, E. *et al.* Low Prolactin and High 20-α-Hydroxysteroid Dehydrogenase Levels Contribute to Lower Progesterone Levels in HIV-Infected Pregnant Women Exposed to Protease Inhibitor–Based Combination Antiretroviral Therapy. *J. Infect. Dis.* **213**, 1532–1540 (2016).
10. Chiasson, M. A. *et al.* Declining HIV/AIDS mortality in New York City. *J. Acquir. Immune Defic. Syndr. 1999* **21**, 59–64 (1999).
11. Palella, F. J. *et al.* Declining morbidity and mortality among patients with advanced human immunodeficiency virus infection. HIV Outpatient Study Investigators. *N. Engl. J. Med.* **338**, 853–860 (1998).

12. Braitstein, P. *et al.* Mortality of HIV-1-infected patients in the first year of antiretroviral therapy: comparison between low-income and high-income countries. *Lancet Lond. Engl.* **367**, 817–824 (2006).

13. World Health Organization. GHO | By category | Prevention of mother-to-child transmission - Estimates by WHO region. *WHO* https://apps.who.int/gho/data/view.main.23500REG (2018).

14. Katlama, C. *et al.* Safety and efficacy of lamivudine-zidovudine combination therapy in antiretroviral-naive patients. A randomized controlled comparison with zidovudine monotherapy. Lamivudine European HIV Working Group. *JAMA* **276**, 118–125 (1996).

15. Fischl, M. A. *et al.* The efficacy of azidothymidine (AZT) in the treatment of patients with AIDS and AIDS-related complex. A double-blind, placebo-controlled trial. *N. Engl. J. Med.* **317**, 185–191 (1987).

16. Vanpouille, C. *et al.* A new antiviral: chimeric 3TC-AZT phosphonate efficiently inhibits HIV-1 in human tissues ex vivo. *Antiviral Res.* **109**, 125–131 (2014).

17. Esser, S., Helbig, D., Hillen, U., Dissemond, J. & Grabbe, S. Side effects of HIV therapy. *JDDG J. Dtsch. Dermatol. Ges.* **5**, 745–754 (2007).

18. Portsmouth, S. D. & Scott, C. J. The renaissance of fixed dose combinations: Combivir. *Ther. Clin. Risk Manag.* **3**, 579–583 (2007).

19. Bushman, F., Landau, N. & Emini, E. New developments in the biology and treatment of HIV. *Proc. Natl. Acad. Sci.* **95**, 11041-11042 (1998).

20. Quercia, R. *et al.* Twenty-Five Years of Lamivudine: Current and Future Use for the Treatment of HIV-1 Infection. *J. Acquir. Immune Defic. Syndr. 1999* **78**, 125–135 (2018).

21. Gulick, R. M. *et al.* Treatment with Indinavir, Zidovudine, and Lamivudine in Adults with Human Immunodeficiency Virus Infection and Prior Antiretroviral Therapy. *N. Engl. J. Med.* **337**, 734–739 (1997).

22. Gulick, R. M. *et al.* 3-year suppression of HIV viremia with indinavir, zidovudine, and lamivudine. *Ann. Intern. Med.* **133**, 35–39 (2000).

23. Portsmouth, S. *et al.* Treatment of primary HIV-1 infection with nonnucleoside reverse transcriptase inhibitor-based therapy is effective and well tolerated. *HIV Med.* **5**, 26–29 (2004).

24. Mandelbrot, L. *et al.* Lamivudine-Zidovudine Combination for Prevention of Maternal-Infant Transmission of HIV-1. *JAMA* **285**, 2083–2093 (2001).

25. Divi, R. L. *et al.* Mitochondrial damage and DNA depletion in cord blood and umbilical cord from infants exposed in utero to Combivir. *AIDS Lond. Engl.* **18**, 1013–1021 (2004).

26. Arnaudo, E. *et al.* Depletion of muscle mitochondrial DNA in AIDS patients with zidovudine-induced myopathy. *Lancet Lond. Engl.* **337**, 508–510 (1991).

27. Brinkman, K., ter Hofstede, H. J., Burger, D. M., Smeitink, J. A. & Koopmans, P. P. Adverse effects of reverse transcriptase inhibitors: mitochondrial toxicity as common pathway. *AIDS Lond. Engl.* **12**, 1735–1744 (1998).

28. Escobar, P. A. *et al.* Genotoxicity assessed by the comet and GPA assays following in vitro exposure of human lymphoblastoid cells (H9) or perinatal exposure of mother-child pairs to AZT or AZT-3TC. *Environ. Mol. Mutagen.* **48**, 330–343 (2007).

29. Tripathi, D. N., Pawar, A. A., Vikram, A., Ramarao, P. & Jena, G. B. Use of the alkaline comet assay for the detection of transplacental genotoxins in newborn mice. *Mutat. Res.* **653**, 134–139 (2008).

30. Bialkowska, A. *et al.* Oxidative DNA damage in fetal tissues after transplacental exposure to 3'-azido-3'-deoxythymidine (AZT). *Carcinogenesis* **21**, 1059–1062 (2000).

31. Meng, Q. *et al.* Zidovudine–didanosine coexposure potentiates DNA incorporation of zidovudine and mutagenesis in human cells. *Proc. Natl. Acad. Sci.* **97**, 12667–12671 (2000).

32. Meng, Q., Su, T., O'Neill, J. P. & Walker, V. E. Molecular analysis of mutations at the HPRT and TK loci of human lymphoblastoid cells after combined treatments with 3'-azido-3'-deoxythymidine and 2',3'-dideoxyinosinedagger. *Environ. Mol. Mutagen.* **39**, 282–295 (2002).

33. de Moraes Filho, A. V. *et al.* Genotoxic and Cytotoxic Effects of Antiretroviral Combinations in Mice Bone Marrow. *PLoS ONE* **11**, (2016).

34. Torres, S. M. *et al.* Mutagenicity of zidovudine, lamivudine, and abacavir following in vitro exposure of human lymphoblastoid cells or in utero exposure of CD-1 mice to single agents or drug combinations. *Environ. Mol. Mutagen.* **48**, 224–238 (2007).

35. Olivero, O. A. *et al.* Transplacental effects of 3'-azido-2',3'-dideoxythymidine (AZT): tumorigenicity in mice and genotoxicity in mice and monkeys. *J. Natl. Cancer Inst.* **89**, 1602–1608 (1997).

36. Walker, D. M. *et al.* Transplacental carcinogenicity of 3'-azido-3'-deoxythymidine in B6C3F1 mice and F344 rats. *Environ. Mol. Mutagen.* **48**, 283–298 (2007).

37. Hleyhel, M. *et al.* Risk of cancer in children exposed to antiretroviral nucleoside analogues in utero: The french experience. *Environ. Mol. Mutagen.* **60**, 404–409 (2019).

38. Hanson, I. C. *et al.* Lack of tumors in infants with perinatal HIV-1 exposure and fetal/neonatal exposure to zidovudine. *J. Acquir. Immune Defic. Syndr. Hum. Retrovirology Off. Publ. Int. Retrovirology Assoc.* **20**, 463–467 (1999).

39. Hankin, C., Lyall, H., Peckham, C. & Tookey, P. Monitoring death and cancer in children born to HIV-infected women in England and Wales: use of HIV surveillance and national routine data. *AIDS Lond. Engl.* **21**, 867–869 (2007).

40. UNAIDS. Women and HIV — A spotlight on adolescent girls and young women. (2019). https://www.unaids.org/en/resources/documents/2019/women-and-hiv.

41. AIDSinfo | UNAIDS. People living with HIV receiving ART. (2019). http://aidsinfo.unaids.org/.

42. Loutfy, M. R. *et al.* Fertility Desires and Intentions of HIV-Positive Women of Reproductive Age in Ontario, Canada: A Cross-Sectional Study. *PLoS ONE* **4**, (2009).

43. Finocchario-Kessler, S. *et al.* Understanding high fertility desires and intentions among a sample of urban women living with HIV in the United States. *AIDS Behav.* **14**, 1106–1114 (2010).

44. Loutfy, M. *et al.* No. 354-Canadian HIV Pregnancy Planning Guidelines. *J. Obstet. Gynaecol. Can.* **40**, 94–114 (2018).

45. WHO. Consolidated guideline on sexual and reproductive health and rights of women living with HIV. (2017). http://www.who.int/reproductivehealth/publications/gender_rights/srhr-women-hiv/en/.

46. World Health Organization (Geneva). *Antiretroviral drugs for treating pregnant women and preventing HIV infection in infant: towards universal access: recommendations for a public health approach*. (2006).

47. World Health Organization. *Guidance on global scale-up of the prevention of mother-to-child transmission of HIV: Towards universal access for women, infants and young children and eliminating HIV and AIDS among children*. (2007).

48. WHO | Consolidated guidelines on the use of antiretroviral drugs for treating and preventing HIV infection. (2016). http://www.who.int/hiv/pub/arv/arv-2016/en/.

49. Else, L. J., Taylor, S., Back, D. J. & Khoo, S. H. Pharmacokinetics of antiretroviral drugs in anatomical sanctuary sites: the fetal compartment (placenta and amniotic fluid). *Antivir. Ther.* **16**, 1139–1147 (2011).

50. Reinhard, G., Noll, A., Schlebusch, H., Mallmann, P. & Ruecker, A. V. Shifts in the TH1/TH2 balance during human pregnancy correlate with apoptotic changes. *Biochem. Biophys. Res. Commun.* **245**, 933–938 (1998).

51. Osakwe, C. E. *et al.* TH1/TH2 cytokine levels as an indicator for disease progression in human immunodeficiency virus type 1 infection and response to antiretroviral therapy. *Roum. Arch. Microbiol. Immunol.* **69**, 24–34 (2010).

52. Fiore, S. *et al.* Antiretroviral therapy-associated modulation of Th1 and Th2 immune responses in HIV-infected pregnant women. *J. Reprod. Immunol.* **70**, 143–150 (2006).

53. Chen, J. Y. *et al.* Highly Active Antiretroviral Therapy and Adverse Birth Outcomes Among HIV-Infected Women in Botswana. *J. Infect. Dis.* **206**, 1695–1705 (2012).

54. Mohammadi, H. *et al.* HIV antiretroviral exposure in pregnancy induces detrimental placenta vascular changes that are rescued by progesterone supplementation. *Sci. Rep.* **8**, (2018).

55. Papp, E. *et al.* HIV Protease Inhibitor Use During Pregnancy Is Associated With Decreased Progesterone Levels, Suggesting a Potential Mechanism Contributing to Fetal Growth Restriction. *J. Infect. Dis.* **211**, 10–18 (2015).

56. Papp, E. *et al.* Low Prolactin and High 20-α-Hydroxysteroid Dehydrogenase Levels Contribute to Lower Progesterone Levels in HIV-Infected Pregnant Women Exposed to Protease Inhibitor–Based Combination Antiretroviral Therapy. *J. Infect. Dis.* **213**, 1532–1540 (2016).

57. Balogun, K. A. *et al.* Elevated Levels of Estradiol in Human Immunodeficiency Virus–Infected Pregnant Women on Protease Inhibitor–Based Regimens. *Clin. Infect. Dis.* **66**, 420–427 (2018).

58. McDonald, C. R. *et al.* Estradiol Levels Are Altered in Human Immunodeficiency Virus–Infected Pregnant Women Randomized to Efavirenz-Versus Lopinavir/Ritonavir-Based Antiretroviral Therapy. *Clin. Infect. Dis.* **66**, 428–436 (2018).

59. Gore, A. C. Developmental programming and endocrine disruptor effects on reproductive neuroendocrine systems. *Front. Neuroendocrinol.* **29**, 358–374 (2008).

60. Bujan, L. *et al.* Decreased semen volume and spermatozoa motility in HIV-1-infected patients under antiretroviral treatment. *J. Androl.* **28**, 444–452 (2007).

61. Pavili, L. *et al.* Decrease of mitochondrial DNA level in sperm from patients infected with human immunodeficiency virus-1 linked to nucleoside analogue reverse transcriptase inhibitors. *Fertil. Steril.* **94**, 2151–2156 (2010).

62. Nicopoullos, J. D. M., Almeida, P., Vourliotis, M. & Gilling-Smith, C. A decade of the sperm-washing programme: correlation between markers of HIV and seminal parameters. *HIV Med.* **12**, 195–201 (2011).

63. Barboza, J. M. *et al.* Use of atomic force microscopy to reveal sperm ultrastructure in HIV-patients on highly active antiretroviral therapy. *Arch. Androl.* **50**, 121–129 (2004).

64. López, S. *et al.* Mitochondrial DNA depletion in oocytes of HIV-infected antiretroviral-treated infertile women. *Antivir. Ther.* **13**, 833–838 (2008).

65. Marston, M. *et al.* Measuring the Impact of Antiretroviral Therapy Roll-Out on Population Level Fertility in Three African Countries. *PLoS ONE* **11**, (2016).

66. Mbita, G., Renju, J., Lija, G., Conserve, D. F. & Todd, J. Effect of antiretroviral therapy on fertility rate among women living with HIV in Tabora, Tanzania: An historical cohort study. *PLOS ONE* **14**, e0222173 (2019).

67. Tweya, H. *et al.* Incidence of Pregnancy Among Women Accessing Antiretroviral Therapy in Urban Malawi: A Retrospective Cohort Study. *AIDS Behav.* **17**, 471–478 (2013).

68. Makumbi, F. E. *et al.* Associations between HIV Antiretroviral Therapy and the Prevalence and Incidence of Pregnancy in Rakai, Uganda. *AIDS Research and Treatment* vol. 2011 e519492 https://www.hindawi.com/journals/art/2011/519492/ (2011).

69. Kim, M. & Costello, J. DNA methylation: an epigenetic mark of cellular memory. *Exp. Mol. Med.* **49**, e322–e322 (2017).

70. Smallwood, S. A. & Kelsey, G. De novo DNA methylation: a germ cell perspective. *Trends Genet.* **28**, 33–42 (2012).

71. Delo, D. M., De Coppi, P., Bartsch, G. & Atala, A. Amniotic fluid and placental stem cells. *Methods Enzymol.* **419**, 426–438 (2006).

72. Haertle, L. *et al.* Hypermethylation of the non-imprinted maternal MEG3 and paternal MEST alleles is highly variable among normal individuals. *PLoS ONE* **12**, (2017).

73. Piedrahita, J. A. The role of imprinted genes in fetal growth abnormalities. *Birt. Defects Res. A. Clin. Mol. Teratol.* **91**, 682–692 (2011).

74. Esteves, S. C. A clinical appraisal of the genetic basis in unexplained male infertility. *J. Hum. Reprod. Sci.* **6**, 176–182 (2013).

75. Pliushch, G. *et al.* Extreme methylation values of imprinted genes in human abortions and stillbirths. *Am. J. Pathol.* **176**, 1084–1090 (2010).

76. Menezo, Y., Dale, B. & Elder, K. The negative impact of the environment on methylation/epigenetic marking in gametes and embryos: A plea for action to protect the fertility of future generations. *Mol. Reprod. Dev.* **86**, 1273–1282 (2019).

77. Page, S. L. & Hawley, R. S. Chromosome choreography: the meiotic ballet. *Science* **301**, 785–789 (2003).

78. Hassold, T. & Hunt, P. To err (meiotically) is human: the genesis of human aneuploidy. *Nat. Rev. Genet.* **2**, 280–291 (2001).

79. Nature Education. Meiosis. *Scitable by Nature Education.* (2004).

80. Gunasegaran, J. P. *Textbook of Histology and A Practical guide, 4e-E-book*. El*sevier Health Sciences.* (2020).

81. Reed, B. G. & Carr, B. R. The Normal Menstrual Cycle and the Control of Ovulation. In *Endotext* (eds. Feingold, K. R. et al.) (MDText.com, Inc., 2000).

82. Conti, M. & Chang, R. J. Chapter 125 - Folliculogenesis, Ovulation, and Luteogenesis. in *Endocrinology: Adult and Pediatric (Seventh Edition)* (eds. Jameson, J. L. et al.) 2179-2191.e3 (W.B. Saunders, 2016).

83. Baerwald, A. R., Adams, G. P. & Pierson, R. A. Ovarian antral folliculogenesis during the human menstrual cycle: a review. *Hum. Reprod. Update* **18**, 73–91 (2012).

84. Gilbert, S. F. Oogenesis. *Dev. Biol. 6th Ed.* (2000).

85. Olivero, O. A. Mechanisms of genotoxicity of nucleoside reverse transcriptase inhibitors. *Environ. Mol. Mutagen.* **48**, 215–223 (2007).

86. Fenech, M. Micronuclei and their association with sperm abnormalities, infertility, pregnancy loss, pre-eclampsia and intra-uterine growth restriction in humans. *Mutagenesis* **26**, 63–67 (2011).

87. Keefe, D. L. *et al.* Telomere length predicts embryo fragmentation after in vitro fertilization in women--toward a telomere theory of reproductive aging in women. *Am. J. Obstet. Gynecol.* **192**, 1256–1260; discussion 1260-1261 (2005).

88. Scheffer, G. J. *et al.* The number of antral follicles in normal women with proven fertility is the best reflection of reproductive age. *Hum. Reprod. Oxf. Engl.* **18**, 700–706 (2003).

89. Scheffer, G. J. *et al.* Antral follicle counts by transvaginal ultrasonography are related to age in women with proven natural fertility. *Fertil. Steril.* **72**, 845–851 (1999).

90. Deanesly, R. The Corpora Lutea of the Mouse, with Special Reference to Fat Accumulation during the Oestrous Cycle. *Proc. R. Soc. Lond. Ser. B Contain. Pap. Biol. Character* **106**, 578–595 (1930).

91. Adibmoradi, M., Morovvati, H. & Moradi, H. Protective Effects of Wheat Sprout on Testicular Toxicity in Male Rats Exposed to Lead. *Reprod. Syst. Sex. Disord.* **04**, (2015).

92. Ogbuewu, I. P., Okoli, I. C. & Uwaezuoke Iloeje, M. Semen quality characteristics, reaction time, testis weight and seminiferous tubule diameter of buck rabbits fed neem (Azadirachta indica A. Juss) leaf meal based diets. *Int. J. Reprod. Biomed.* **7**, 23–0 (2009).

93. Lanning, L. L. *et al.* Recommended approaches for the evaluation of testicular and epididymal toxicity. *Toxicol. Pathol.* **30**, 507–520 (2002).

94. McCoard, S. A., Lunstra, D. D., Wise, T. H. & Ford, J. J. Specific Staining of Sertoli Cell Nuclei and Evaluation of Sertoli Cell Number and Proliferative Activity in Meishan and White Composite Boars During the Neonatal Period. *Biol. Reprod.* **64**, 689–695 (2001).

95. Kalantari Hesari, A., Shahrooz, R., Ahmadi, A., Malekinejad, H. & Saboory, E. Crocin prevention of anemia-induced changes in structural and functional parameters of mice testes. *J. Appl. Biomed.* **13**, 213–223 (2015).

96. Razi, M. *et al.* Histological and histochemical effects of Gly-phosate on testicular tissue and function. *Iran. J. Reprod. Med.* **10**, 181–192 (2012).

97. Smith, L. B. & Walker, W. H. The Regulation of Spermatogenesis by Androgens. *Semin. Cell Dev. Biol.* **0**, 2–13 (2014).

98. Marchiani, S., Tamburrino, L., Muratori, M. & Baldi, E. Epididymal Sperm Transport and Fertilization. in *Endocrinology of the Testis and Male Reproduction* (eds. Simoni, M. & Huhtaniemi, I. T.) 457–478 (Springer International Publishing, 2017).

99. Dyson, A. L. & Orgebin-Crist, M. C. Effect of hypophysectomy, castration and androgen replacement upon the fertilizing ability of rat epididymal spermatozoa. *Endocrinology* **93**, 391–402 (1973).

100. Ayuob, N., Al-Harbi, M. & Abdulhadi, S. Is the Chronic Use of Ferula Harmonis to Enhance Mice Erectile Function Effective and Safe? A Histopathological Study. *Syst. Biol. Reprod. Med.* **60**, 282-292 (2014).

101. Choi, H. *et al.* Reduced Fertility and Altered Epididymal and Sperm Integrity in Mice Lacking ADAM7. *Biol. Reprod.* **93**, (2015).

102. Greaves, P. Chapter 11 - Male Genital Tract. in *Histopathology of Preclinical Toxicity Studies (Fourth Edition)* (ed. Greaves, P.) 615–666 (Academic Press, 2012).

103. Wang, L., Kourtis, A. P., Ellington, S., Legardy-Williams, J. & Bulterys, M. Safety of tenofovir during pregnancy for the mother and fetus: a systematic review. *Clin. Infect. Dis. Off. Publ. Infect. Dis. Soc. Am.* **57**, 1773–1781 (2013).

104. Seier, T., Zilberberg, G., Zeiger, D. M. & Lovett, S. T. Azidothymidine and other chain terminators are mutagenic for template-switch-generated genetic mutations. *Proc. Natl. Acad. Sci. U. S. A.* **109**, 6171–6174 (2012).

105. Sabatinos, S. A., Mastro, T. L., Green, M. D. & Forsburg, S. L. A mammalian-like DNA damage response of fission yeast to nucleoside analogs. *Genetics* **193**, 143–157 (2013).

106. Hayles, J. & Nurse, P. Introduction to Fission Yeast as a Model System. *Cold Spring Harb. Protoc.* **2018**, (2018).

107. Sabatinos, S. A. & Forsburg, S. L. Molecular genetics of Schizosaccharomyces pombe. *Methods Enzymol.* **470**, 759–795 (2010).

108. Botstein, D. & Fink, G. R. Yeast: an experimental organism for modern biology. *Science* **240**, 1439–1443 (1988).

109. Hoffman, C. S., Wood, V. & Fantes, P. A. An Ancient Yeast for Young Geneticists: A Primer on the Schizosaccharomyces pombe Model System. *Genetics* **201**, 403–423 (2015).

110. Murakami, H. & Nurse, P. DNA replication and damage checkpoints and meiotic cell cycle controls in the fission and budding yeasts. *Biochem J.* **349**, 1-12 (2000).

111. Alcasabas, A. A. *et al.* Mrc1 transduces signals of DNA replication stress to activate Rad53. *Nat. Cell Biol.* **3**, 958–965 (2001).

112. Barnum, K. J. & O'Connell, M. J. Cell cycle regulation by checkpoints. *Methods Mol. Biol. Clifton NJ* **1170**, 29–40 (2014).

113. Nyberg, K. A., Michelson, R. J., Putnam, C. W. & Weinert, T. A. Toward maintaining the genome: DNA damage and replication checkpoints. *Annu. Rev. Genet.* **36**, 617–656 (2002).

114. Capasso, H. *et al.* Phosphorylation activates Chk1 and is required for checkpoint-mediated cell cycle arrest. *J. Cell Sci.* **115**, 4555–4564 (2002).

115. GraphPad Prism 8 User Guide - Box and whiskers graphs. https://www.graphpad.com/guides/prism/8/user-guide/box-and-whiskers.htm.

116. VassarStats: Statistical Computation Web Site. http://vassarstats.net/.

117. Fantes, P. A. & Creanor, J. Canavanine resistance and the mechanism of arginine uptake in the fission yeast Schizosaccharomyces pombe. *J. Gen. Microbiol.* **130**, 3265–3273 (1984).

118. Sabatinos, S. A. & Forsburg, S. L. Preserving the Replication Fork in Response to Nucleotide Starvation: Evading the Replication Fork Collapse Point. *Mech. DNA Replication* (2013) doi:10.5772/51393.

119. Hall, B. M., Ma, C.-X., Liang, P. & Singh, K. K. Fluctuation AnaLysis CalculatOR: a web tool for the determination of mutation rate using Luria–Delbrück fluctuation analysis. *Bioinformatics* **25**, 1564–1565 (2009).

120. Foster, P. L. Methods for Determining Spontaneous Mutation Rates. *Methods Enzymol.* **409**, 195–213 (2006).

121. Fantes, P. & Nurse, P. Control of cell size at division in fission yeast by a growth-modulated size control over nuclear division. *Exp. Cell Res.* **107**, 377–386 (1977).

122. Mansky, L. M. & Bernard, L. C. 3'-Azido-3'-Deoxythymidine (AZT) and AZT-Resistant Reverse Transcriptase Can Increase the In Vivo Mutation Rate of Human Immunodeficiency Virus Type 1. *J. Virol.* **74**, 9532–9539 (2000).

123. Mansky, L. M., Pearl, D. K. & Gajary, L. C. Combination of Drugs and Drug-Resistant Reverse Transcriptase Results in a Multiplicative Increase of Human Immunodeficiency Virus Type 1 Mutant Frequencies. *J. Virol.* **76**, 9253–9259 (2002).

124. Sanne, I., Smego, R. A. & Mendelow, B. V. Systematic review of combination antiretroviral therapy with didanosine plus hydroxyurea: A partial solution to africa's HIV/AIDS problem? *Int. J. Infect. Dis.* **5**, 43–48 (2001).

125. Kucsera, J., Yarita, K. & Takeo, K. Simple detection method for distinguishing dead and living yeast colonies. *J. Microbiol. Methods* **41**, 19–21 (2000).

126. Chan, S. S. L. *et al.* Mitochondrial toxicity in hearts of CD-1 mice following perinatal exposure to AZT, 3TC, or AZT/3TC in combination. *Environ. Mol. Mutagen.* **48**, 190–200 (2007).

127. Tilly, J. Ovarian follicle counts – not as simple as 1, 2, 3. *Reprod. Biol. Endocrinol.* 1-11 (2003).

128. Myers, M., Britt, K. L., Wreford, N. G. M., Ebling, F. J. P. & Kerr, J. B. Methods for quantifying follicular numbers within the mouse ovary. *Reprod. Camb. Engl.* **127**, 569–580 (2004).

129. Gray, R. H. *et al.* Population-based study of fertility in women with HIV-1 infection in Uganda. *Lancet Lond. Engl.* **351**, 98–103 (1998).

130. Komatsu, K. & Masubuchi, S. The concentration-dependent effect of progesterone on follicle growth in the mouse ovary. *J. Reprod. Dev.* **63**, 271–277 (2017).

131. Rebourcet, D. *et al.* Sertoli Cell Number Defines and Predicts Germ and Leydig Cell Population Sizes in the Adult Mouse Testis. *Endocrinology* **158**, 2955–2969 (2017).

132. Rebourcet, D. *et al.* Sertoli cells maintain Leydig cell number and peritubular myoid cell activity in the adult mouse testis. *PloS One* **9**, e105687 (2014).

133. Rietschel, P. *et al.* Prevalence of hypogonadism among men with weight loss related to human immunodeficiency virus infection who were receiving highly active antiretroviral therapy. *Clin. Infect. Dis. Off. Publ. Infect. Dis. Soc. Am.* **31**, 1240–1244 (2000).

134. Newshan, G., Taylor, B. & Gold, R. Sexual functioning in ambulatory men with HIV/AIDS. *Int. J. STD AIDS* **9**, 672–676 (1998).

135. Osadchuk, L. V. Spermatogenesis parameters and testosterone production at puberty as predictors of testicular functional activity in mice (Mus musculus) *J. Evol. Biochem. Phys.* **52**, 475-481 (2016).

136. De Grava Kempinas, W. & Klinefelter, G. R. Interpreting histopathology in the epididymis. *Spermatogenesis* **4**, (2015).

137. Glasel, J. A. Validity of nucleic acid purities monitored by 260nm/280nm absorbance ratios. *BioTechniques* **18**, 62–63 (1995).

138. Shao, W.-J., Tao, L.-Y., Gao, C., Xie, J.-Y. & Zhao, R.-Q. Alterations in Methylation and Expression Levels of Imprinted Genes H19 and Igf2 in the Fetuses of Diabetic Mice. *Comp. Med.* **58**, 341–346 (2008).